CENTRO DE INVESTIGACIONES
EN OPTICA, A.C.

“SPATIALLY ENCODED QUANTUM STATE FOR APPLICATION IN QUANTUM INFORMATION”

Tesis que para obtener el grado de Maestra en Ciencias (Óptica)

Presenta: Susana Plascencia Orozco

Director de Tesis: Dr. Roberto Ramírez Alarcón

León · Guanajuato · México

Noviembre 2020

Acknowledgments

I would like to express my gratitude to my advisor at CIO, Dr. Roberto Ramírez Alarcón, for allowing me to be part of his group and for the help and advice in many aspects related and unrelated to my thesis project. Also to my advisor at Fraunhofer IOF, Dr. Fabian Steinlechner, for receiving me into his group, for his guidance and patience during my stay, and apart from being a great advisor, he is a great person. I would like to acknowledge my group partners at IOF especially to Carlos Sevilla and Varun Kaipalath, who were my biggest help in my thesis project in the laboratory. Additionally, my all my lovely group colleagues at CIO and IOF as well as my Family, who showed me their support in other ways and had to stand me in my most stressful moments. And finally, but not less important, I would like to thank to Luis Enrique Padilla since without all his unconditional support this achievement would not have been possible.

I am very grateful to CONACYT for granting me a scholarship during my Master studies, along with an additional scholarship (Beca de Movilidad Extranjera 2019) for my six months stay abroad.

ABSTRACT

The spatial structure of light as a degree of freedom holds great potential for encoding large amounts of information in both classical and quantum optical communication systems. Spatial modes such as Hermite Gauss, or Laguerre Gauss modes are embedded in an infinite dimensional Hilbert space, a feature that can significantly enhance quantum information processing protocols. In particular, Laguerre Gauss modes, which are associated with discrete value of orbital angular momentum (OAM), have enabled numerous experimental demonstrations of high-dimensional quantum protocols that exhibit key advantages such as improved noise-tolerance or channel capacity in comparison to two-dimensional qubit state encoding. Quantum states exhibiting orbital momentum entanglement can be generated via spontaneous parametric down conversion (SPDC) in a nonlinear crystal as a consequence of momentum conservation during the process.

This thesis we investigate a two-photon state in space and frequency using a Gaussian pump beam, for SPDC bulk in non-linear crystals, considering a collinear geometry, and restricting the spectral bandwidth to the narrowband case. We derive analytic expressions for two- and single photons spectral brightness. We also investigate the role of focusing parameters. As well as the optimal waist for the pump and the collection modes. A solution for the pair collection efficiency was previously derived in [1]. However, an analytical expression for the single photon collection has not been (to the best of our knowledge) reported, in order to verify that our results are correct, we calculate the heralding efficiency (given by the ratio of pair collection detection and the detection of a single photon) and compare our results with the one reported in [2]. For both (pair- and single-photon) collection probabilities our findings are in excellent agreement with the previous studies. The results obtained in this work are expected to be useful for designing SPDC sources with high performance in multiple categories.

Contents

List of figures

1 Introduction

Quantum communications systems are based on the linearity of quantum theory and the existence of superpositions of quantum bits (qubits) [3]. When multiple qubits exist in a simultaneous superposition state, the system is said to be entangled. The photons that constitute the entangled states are strongly correlated and their entangled nature can be preserved over large distances. The most common source for generating entangled photon pairs is by means of spontaneous parametric down conversion, in which a strong field (pump) interacts with a non-linear crystal, generating a lower frequency photon pair (signal and idler) that propagates at certain angle [4]. When SPDC is properly engineered, the photon pairs can be entangled in any degree of freedom for example path [5], time-bin [6], frequency [7], or spatial modes [8]. The spatial structure of entangled states can be encoded in the orbital angular momentum (OAM) [9], which provides an infinite-dimensional discrete Hilbert space [10]. This characteristic is of interest since it can be used to conduct proof-of-principle demonstrations of quantum protocols whose implementation requires higher-dimensional Hilbert spaces, such as the violation of Bell inequalities with qutrits [8] and the implementation of quantum key distribution (QKD) [11], [12]. The spatial structure of the down-converted bi-photons can be expressed as a superposition of Laguerre–Gauss (LG) modes of different amplitudes, angular and radial momenta, with the width of the modal expansion relating to the amount of entanglement of the final state [13].

In general the efficiency of the photon pairs generated by SPDC is very slow, hence efforts have been made to improve the brightness of the entangled photon sources by exploring different nonlinear crystals in bulk [14], [15] and waveguide [16] structures, different phase-matching geometries including type-II [17], [18], type-I [19] and type-0 [18], [20], [21], and different experimental schemes. Moreover, any experimental detection system collects only part of the total number of the generated pair, for this reason, it is of our interest to maximize the coupling efficiency into the single mode fibers. This single mode coupling efficiency of a pair source is commonly quantified in terms of per-photon probability of collecting a photon pair, the spectral bandwidth, and the probability of collecting a photon pair, conditioned on the collection of a single photon.

Several studies of SPDC [1], [22], [23] have addressed the question of how to focus the pump and/or collection modes, as well as, the proper sizes of the beam waist of these fields for a given crystal length can optimize the probabilities for photon pairs generated by SPDC, and if there is a tradeoff between them. Palacios *et. al*. [1] have derived an analytical solution for the pair-collection probability, where one can easily find the optimal size of the pump and mode collection waist that leads to a maximum value of ~82% under this ideal conditions. The importance of this result lies on the fact that this value is a universal quantity and it is independent of the crystal length. The work of Bennik's [22] gives an extensive analysis restricted to collinear Gaussian modes for the pump field and collected photon for the peak spectral density, photon bandwidths, absolute pair collection probability, heralding ratio, and spectral purity, finding that most of these properties are independent of the crystal length. But more important, he concluded that higher heralding ratios can be achieved, at the cost of significantly reduced brightness, by focusing the modes less tightly.

With regard to these previous studies, in the present thesis we have reproduced the calculation for the two-photons collection probability presented in [1] with the aim of corroborating the optimal parameters achieved in this article and having a better understanding of the role of some parameters such as the crystal length and the focusing parameters. We also have extended the analysis for the single photon collection probability, finding an analytical solution for this quantity. Using the two analytical solutions given by the spectral brightness, we could easily calculate the heralding efficiency and compare our results with previous studies reported on references [2], [22]. Our approach is based on a periodically-poled nonlinear crystal of length L, illumined by a continuous wave pump beam in the collinear configuration for SPDC type II in the narrowband limit. A better understanding and characterization of both properties (spectral brightness and heralding efficiency) are then crucial to the development of future quantum technologies [24], [25].

Chapter 2 gives a brief overview of the spatial modes of light, as well as the relevant concepts for the description of the SPDC process, it also shows the derivation of the main equations that lay in the foundations of our analysis. Chapter 3 shows the analytical and numerical results obtained for single-mode fiber coupling efficiency and spectral properties of SPDC photons after the mode projection, and the discussion regarding our results and

previous studies. Chapter 4 summarizes the major results of this thesis. We provide a brief note on the further experiments we plan to perform using spatial modes of light and a mode sorter. Additional to this, Appendix A presents some experimental configuration for generation and manipulation of the spatial modes.

2 Theory

2.1 Wave equation

From the description of Classical Electrodynamics given by Maxwell's Equations, for the case of no free charges and currents where the quantities $\widetilde{\boldsymbol{E}}$ and $\widetilde{\boldsymbol{H}}$ are given in units of *Volt/m* and *ampere/m* respectively, we have that [26]:

$$\vec{\nabla} \cdot \varepsilon \widetilde{\boldsymbol{E}} = 0, \tag{1}$$

$$\vec{\nabla} \cdot \mu \widetilde{\boldsymbol{H}} = 0, \tag{2}$$

$$\vec{\nabla} \times \widetilde{\boldsymbol{E}} = -\frac{\partial}{\partial t}\left(\mu \widetilde{\boldsymbol{H}}\right), \text{ and} \tag{3}$$

$$\vec{\nabla} \times \widetilde{\boldsymbol{H}} = \frac{\partial}{\partial t}\left(\varepsilon \widetilde{\boldsymbol{E}}\right), \tag{4}$$

Using these equations, we can obtain an expression that describes the propagation of the electromagnetic radiation in a medium. This is well defined by the wave equation [27]:

$$\nabla^2 \boldsymbol{\varphi} - \mu\varepsilon \frac{\partial^2}{\partial t^2} \boldsymbol{\varphi} = 0, \tag{5}$$

where $\boldsymbol{\varphi}$ is a scalar function representing the field amplitude and ε, μ represents the permittivity and permeability, respectively, which are related to the electric and magnetic susceptibilities of the medium, χ_e and χ_m as:

$$\varepsilon = \varepsilon_r \varepsilon_0 = \varepsilon_0(1 + \chi_e), \text{ and} \tag{6}$$

$$\mu = \mu_r \mu_0 = \mu_0(1 + \chi_m), \tag{7}$$

here ε_r and μ_r are the relative permittivity and permeability, respectively.

In case of a linear, homogenous, isotropic medium and a monochromatic wave (i.e. sinusoidal time variations in the fields), if the field is polarized in one component $\tilde{E} = E_i \hat{\mathrm{e}}_i$ it is possible to write it as a product of its spatial temporal components $E_i = T(t)U(r)$. Now if we substitute it in Eq. (5) it is straight forward to show that the temporal dependence of the electric field is:

$$T(t) = e^{i\omega t}, \tag{8}$$

and the spatial dependence part $U(r)$ is the solution of the time independent wave equation or Helmholtz equation given by:

$$\nabla^2 U(r) + k^2 U(r) = 0, \tag{9}$$

where *k* is the propagation constant (or wave number) defined as:

$$k = \frac{\omega}{V} = \omega \frac{n}{c}, \tag{10}$$

here V is the velocity of the propagation of the wave $V = \frac{c}{\sqrt{\epsilon\mu}}$ being *c* the speed of the light. Then, we can express the refraction index as:

$$n = \sqrt{\epsilon\mu}\,. \tag{11}$$

Now, assuming that the propagation of the wave is along the optical axis z and applying the paraxial approximation we can write $U(r)$ as:

$$U(r) = u(r)e^{-ikz}. \tag{12}$$

As a consequence of the paraxial assumption and using the slowly varying envelope approximation, we find that:

$$\left|\frac{\partial^2 u}{\partial z^2}\right| \ll k \left|\frac{\partial u}{\partial z}\right|. \tag{13}$$

Then Eq. (9) becomes [27]:

$$\nabla^2 u(r) - 2ik\frac{\partial u(r)}{\partial z} = 0. \tag{14}$$

The Helmholtz equation in the paraxial regime can find different families of solutions and be solved in different coordinate systems.

2.2 Hermite-Gauss modes

For rectangular coordinates system the solution of the paraxial equation are given by the product of a Gaussian functions and Hermite polynomials and a phase term. The mathematical representation of Hermite-Gaussian modes is [28]:

$$HG_{nm}(x,y,z) = \frac{1}{w(z)}\sqrt{\frac{2^{(1-m-n)}}{\pi n!\, m!}} H_m\left(\frac{\sqrt{2}x}{\omega(z)}\right) H_n\left(\frac{\sqrt{2}y}{\omega(z)}\right) e^{[i(m+n+1)\xi(z)]} \times e^{\frac{-r^2}{w^2(z)}} e^{\frac{-ikr^2}{2R}} e^{-ikz}, \tag{15}$$

where H_m and H_n are Hermite polynomials with n, m positive integers. The Term z_R represents the Raylegh range, $\xi(z)$ is the Gouy phase and $\omega(z)$ the beam size given by:

$$r = \sqrt{x^2 + y^2}, \tag{16}$$

$$\omega(z) = \omega_0 \sqrt{1 + \left(\frac{z}{z_R}\right)^2}, \tag{17}$$

$$\mathrm{R}(z) = z\left[1 + \left(\frac{z_R}{z}\right)^2\right], \tag{18}$$

$$\omega_0 = z\sqrt{\frac{\lambda z_R}{\pi}}, \text{ and} \tag{19}$$

$$\xi(z) = arctan\left(\frac{z}{z_R}\right). \tag{20}$$

Eqs.(18) and (19) describes radius of curvature R(z) and beam waist ω_0 of the paraboloidal wave given by Eq. (15). We can notice that the Gouy phase $e^{[i(m+n+1)]}$ contains information regarding the mode order defined as $N = n + m$.

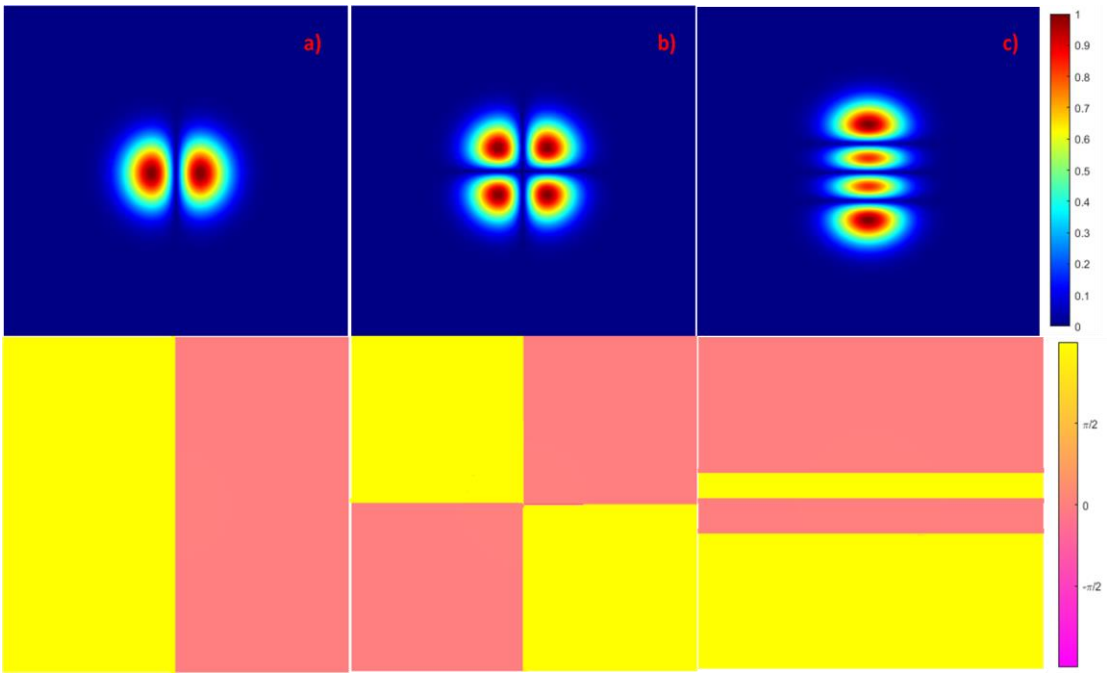

Figure 2.1 Intensity profile: a) HG10, b) HG11, c) HG30 and below them their respective phase profiles of each of these HG modes.

In the Figure 2.1 the intensity and phase profiles for some HG modes are shown. Here the number of lobes in the x-direction is given by $(m + 1)$ and similarly for the y-direction where the modes have $(m + 1)$ lobes.

2.3 Laguerre-Gauss modes

Laguerre-Gaussian modes are the solution of the paraxial Helmholtz Equation in cylindrical coordinate system where this solution is given by the product of a Gaussian function with a generalized Laguerre polynomial as [28]:

$$LG_p^l(\rho,\varphi,z) = \frac{\omega_0}{\omega(z)}\sqrt{\frac{2p!}{\pi(|l|+p)!}}\left(\frac{\sqrt{2}\rho}{w(z)}\right)^{|l|} LG_p^l\left[2\left(\frac{\rho}{w(z)}\right)^2\right] e^{[i(2p+|l|+1)\xi(z)]} \times e^{\frac{-\rho^2}{w^2(z)}} e^{\frac{-ik\rho^2}{2R}} e^{[-il\varphi]}, \quad (21)$$

where LG_p^l is the associated Laguerre polynomial, l is the azimuthal index and p is the radial index. In particular (p, l) are integer numbers with $p \geq 0$ while l can take both positive or negative values. The other variables in eq. (21) were described in the section 2.2. The lowest order of these mode $p = l = 0$ is the Gaussian beam (TEM_{00} mode). Experimentally, both angular (l) and radial (p) momenta are controlled and converted between one another using several methods, being the most common the diffractive optical elements (holograms) displayed by spatial light modulators (SLMs) [See Appendix A].

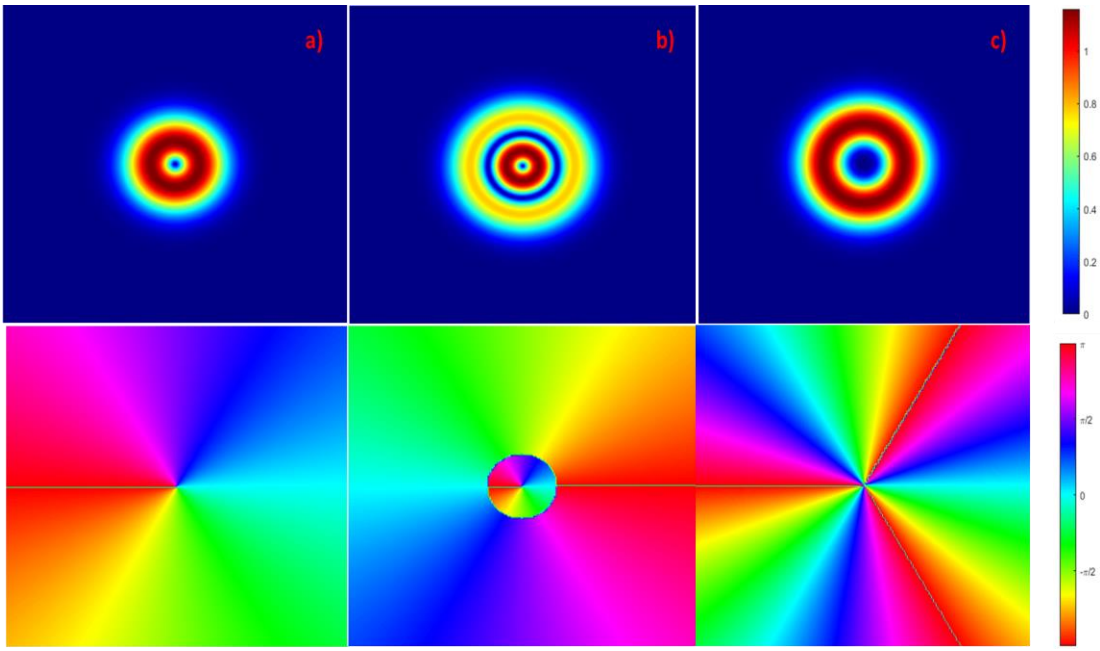

Figure 2.2 Intensity profile and phase of some LG modes: a) LG01, b) LG11, c) LG03 and below their respective phase profile. LG mode intensity cross section, with $l > 0$ comprises p+1 concentric rings with a zero on-axis intensity.

It is well known that light beams with an azimuthal phase dependence of $e^{[-il\varphi]}$, as it is the case of the LG modes, carry an orbital angular momentum (OAM) [29]. The phase front has a helicoidally pattern along the $\hat{z}$ in such a way that the contact between all different phases in the center of the transverse plane causes that the field intensity vanishes, giving rise to a phase singularity. The torque exhibited leads to an optical vortex that it is associated to a number known as topological charge l that refers to the number of twist of the wavefront over a distance. This twisting causes a non-vanishing contribution of the OAM [30]. The intensity and phase profiles of some LG modes are shown in Figure 2.2.

Laguerre-Gaussian modes, as well as Hermite-Gaussian modes, are a complete set of orthonormal modes both in the radial index when it is integrated over ρ, and in the azimuthal index over φ. Mathematically this is expressed as:

$$\int_0^{2\pi} d\varphi \int_0^{\infty} \rho \, d\rho \left[LG_p^l(\rho,\varphi,z)\right]\left[LG_{p'}^{l'}(\rho,\varphi,z)\right]^* = \delta_{pp'}\delta_{ll'} \, . \tag{22}$$

Hermite-Gaussian modes are also orthonormal with an analogous condition as in Eq. (22) but with m and n index, when integrated over x and y, respectively.

2.4 Spontaneous Parametric Down Conversion theory

Spontaneous parametric down-conversion (SPDC) is a non-linear optical process, where a high energetic pump photon of frequency ω_p interacts with a non-linear medium and spontaneously generates a pair of photons of frequency ω_s and ω_i (where the subscripts *p*, *s* and *i* denote pump, signal and idler photons respectively) which have lower energy than the incident photon. Unlike in classical parametric processes, the fields of the photons signal and idler are in their respective vacuum sates (see Figure 2.3.a).

Inasmuch as SPDC is a parametric process the phase matching requirements should be fulfilled, given by the conservation of the energy and momentum as:

$$\Delta\omega = \omega_p - \omega_s - \omega_i \, , \tag{23}$$

$$\Delta k = k_p - k_s - k_i \, . \tag{24}$$

In Eq. (23) energy conservation allows that the decay process to take place in many target modes (showed it in Figure 2.3.c), while Eq.(24) is known as phase-matching since it establishes the geometrical configuration of the SPDC (Figure 2.3.b). This condition should

be satisfied to the conversion takes place into any particular pair of directions. As a result of these conditions the created photons are strongly correlated in frequency and direction of emission.

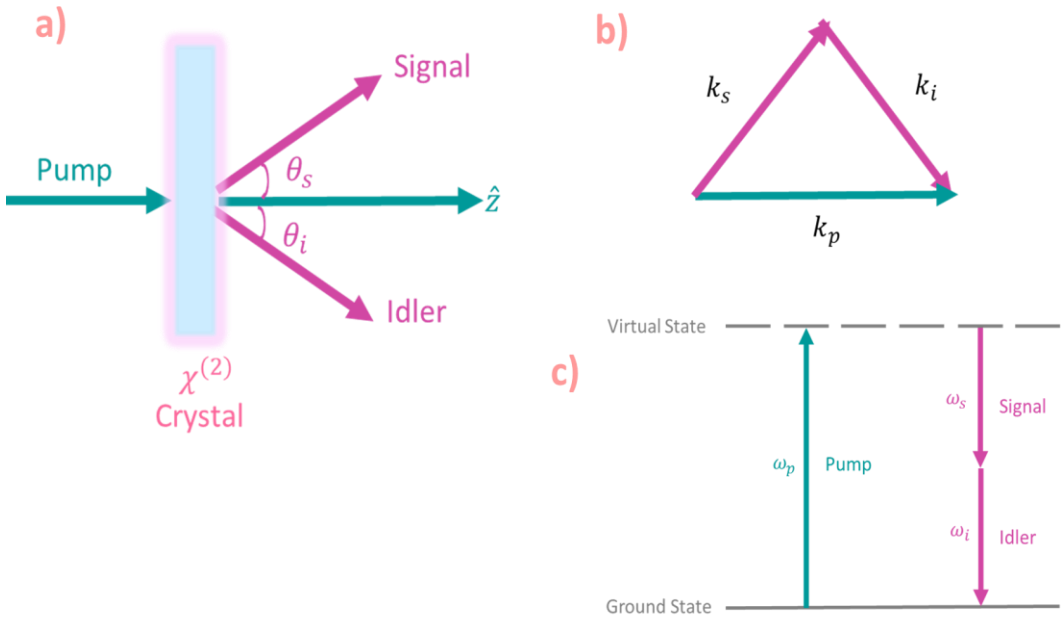

Figure 2.3 Sketch of the SPDC process. a) A Guassian pump propagating in the z axis incised on a non-linear crystal producing a pair of photons at angles θ_s and θ_i to the pump propagation's direction. b) Conservation of momentum and c) conservation of the energy

2.4.1 Phase matching

Ideally the case that satisfies Eq. (24) for an efficient non-linear parametric process is reached when $\Delta k = 0$, the requirement for this condition to be fulfilled is:

$$k_1 + k_2 = k_3 = \frac{n_3\omega_3}{c} = \frac{n_1\omega_1}{c} + \frac{n_2\omega_2}{c}, \tag{25}$$

which is not realistic in most of the materials due to the normal dispersion $n_1(\omega_1) < n_2(\omega_2) < n_3(\omega_3)$. The refraction index decays when the wavelength increases in the transparent regime. Nevertheless, birefringent materials [31] which have different refractive indices along different symmetry axes (two in the case of the uniaxial crystal or three for biaxial crystals) can be used to satisfy this condition. Uniaxial crystals are characterized by a particular direction named optical axis (z axis). When the polarization of the light propagating is perpendicular to the plane containing the vector $\boldsymbol{k}$ and the optical axis, it is called ordinary polarization. On the other hand, if the light propagates with its polarization

perpendicular to the ordinary ray (polarization direction parallel to the optical axis) it is called extraordinary polarization and the refractive index depends on the angle between ***k*** and the optical axis as:

$$\frac{1}{n_e(\theta)^2} = \frac{sin^2(\theta)}{\bar{n}_e^2}\frac{cos^2(\theta)}{n_o^2}, \tag{26}$$

where $\bar{n}_e$ is the principal value of the extraordinary refractive index. In order to satisfy the phase matching condition, the angle θ must be adjusted till $n_e(\theta)$ reaches $\Delta k = 0$. Depending on the polarization direction of the pump with respect of the optical axis and ***k*** vector (as we describe above) we will have different configuration for SPDC. For the first configuration called type-0, the pump photon, as well as, generated pair (signal and idler) have the same polarization, either ordinary or extraordinary. In the second configuration (type-I) the generated pair of photons can be propagated collinear or non-collinear satisfying the phase matching conditions and the pair photons will have the same polarization but opposite to the polarization direction of the pump. In this configuration the photons signal and idler possess the same refractive index and thus lie on the same cone Figure 2.4.

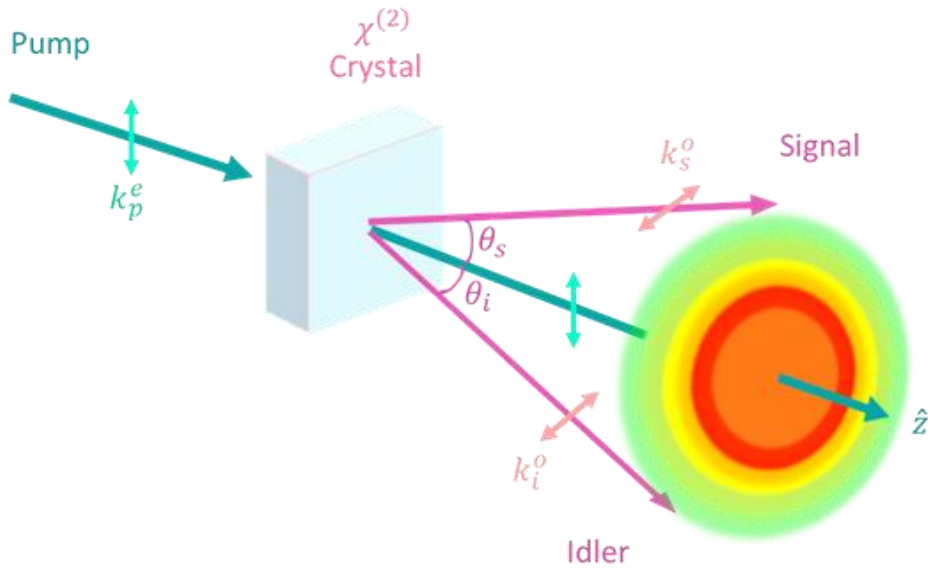

Figure 2.4 SPDC type-I: degenerate, non-collinear case, idler and signal cone are identical.

In Figure 2.4, the generated case is shown, where the wavelength of the photons pair are double the pump wavelength, by changing the angle of the pump with respect to the crystal the emission the cone changes its size. For the third configuration of SPDC (type-II) the

photons pairs signal and idler have orthogonal polarizations, provoking that the cones created by the two photons be not coaxial as a consequence of the different refractive index of the signal and idler photons (see Figure 2.5). Table 2.1 exemplify the SPDC configuration describe above.

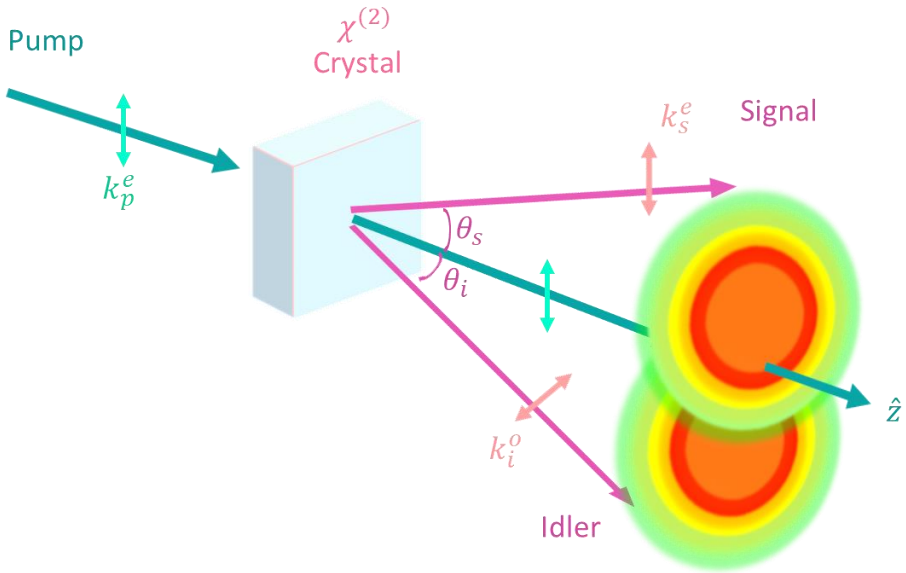

Figure 2.5 SPDC type-II: degenerate, non-collinear case, idler and signal with non-coaxial cone.

The apertures of the cone are given by the emission angles $\theta_{s,i}$ associated to the frequencies $\omega_{s,i}$. In degenerate SPDC, both photons are emitted at the same angle $\theta_s = \theta_i$ and the cones overlap. There are two cases of degenerated SPDC: the collinear in which the aperture of the cones tends to zero due to the photons pair propagation is parallel to the pump, and the non-collinear case in which the signal and idler photons are not parallel to the pump that is the case exemplify in Figure 2.4 and Figure 2.5.

Table 2.1 Refraction index of each photon (pump, signal and idler) for different SPDC type. In this table we assume that the pump polarization is in the extraordinary direction.

SPDC type	*Pump*	*Signal*	*Idler*
Type-0	n_e	n_e	n_e
Type-1	n_e	n_o	n_o
Type-2	n_e	n_o	n_e

When the condition of perfect phase matching $\Delta k = 0$ cannot be satisfied, it is possible to reach phase matching by considering the formation of layers with alternate orientation in a birefringent material, called periodical poling [27], then the mismatching factor reads:

$$\Delta k = k_p - k_s - k_i - \frac{2\pi}{\Lambda}, \tag{27}$$

where Λ is the poling period. Even though the phase matching condition defines the main characteristics of the generated two-photon state, it is necessary to consider other important factors that allow us to have a better understanding of this phenomena, such as a description of the mathematical model that give us information about the quantum state evolution inside the medium, considering the spatial structure of the pump beam and at the generated pair, the properties of the crystal, as well as, the detection system. The next section describes the two-photon state mathematically, taking into account all these factors.

2.4.2 Classical non-linear description

The susceptibilities χ_e and χ_m defined in Eqs. (6) and (7),respectively, can be spatial and frequency dependent. They describe the medium response to the interaction with an external electromagnetic field. This interaction is in the form of an induced polarization $\tilde{P}$ or magnetization, $\widetilde{M}$ as:

$$\tilde{P} = \epsilon_0 \chi_e \widetilde{E}\,, \tag{28}$$

$$\widetilde{M} = \chi_m \widetilde{M}\,. \tag{29}$$

For small field amplitudes, the polarization is approximately linear. We can find a general expression for the induced polarization by expanding it in a power series to consider the non-linear contributions of the electric field as [31]:

$$\tilde{P}(t) = \epsilon_0\left[\chi^{(1)}\tilde{E}(t) + \chi^{(2)}\tilde{E}^{(2)}(t) + \chi^{(3)}\tilde{E}^{(3)}(t) + \cdots\right], \tag{30}$$

where $\chi^{(1)}$ represents the linear susceptibility and $\chi^{(2)}, \chi^{(3)}$ are the second and third order non-linear susceptibilities, respectively.

As we mention before Eq. (28) is the result of a small field amplitude that allows us to neglect the rest of the terms in Eq. (30). However, when the amplitudes of the electric field increases, the higher order terms in the induced polarization become relevant, in such way that a non-linear responds of the material to the field appears. Some optical non-linear processes resulting from these interactions include for example, Kerr effect, harmonics generation, frequency generation, Raman scattering [31].

The non-linear polarization of second order (non-linear) process according to Eq. (30) is given by:

$$\tilde{P}^{(2)}(t) = \epsilon_0\chi^{(2)}\tilde{E}^{(2)}(t). \tag{31}$$

Non-linear processes are highly inefficient, being $\chi^{(2)}$ of the order of 10^{-12}. Therefore an intense electric field is needed to observe non-linear optical phenomena and they are only present in non-centrosymmetric media, where, the electronic potential is not symmetric. Under these assumptions and considering propagating waves of the form:

$$\tilde{E}_n(r,t) = \tilde{A}_n(r)e^{i(k_n z - \omega_n t)} + c.c \tag{32}$$

where c.c is the complex conjugate term and $k_n = \frac{n_n\omega_n}{c}$ with $n_n^2 = \varepsilon^{(1)}(\omega_n)$ where the upper index (1) is the linear part only. If we consider a three wave interaction only [32], [33], which is the case of the non-linear process of SPDC as well as Second Harmonic Generation (SHG) we will only take into account the first non-linear for the polarization given by:

$$P_i^{NL} = \varepsilon_0 \sum_j \sum_k \chi_{ijk}^{(2)} E_j E_k, \tag{33}$$

with $\{i,j,k\} = \{x,y,z\}$ and $\chi_{ijk}^{(2)}$ the second order term non-linear susceptibility of the medium. Substituting Eqs. (32) and (33) into the wave equation $\vec{\nabla}^2\tilde{E} - \frac{1}{c^2}\frac{\partial^2\tilde{E}}{\partial t^2} = \frac{1}{\varepsilon_0 c^2}\frac{\partial^2\tilde{P}}{\partial t^2}$ we can get the following equation:

$$\frac{d^2A_3}{dz^2} + 2ik_3\frac{dA_3}{dz} = -\frac{4d_{eff}\omega_3}{c^2}A_1A_2e^{iz(k_1+k_2-k_3)}, \tag{34}$$

where $d_{eff} = \frac{1}{2}\chi_{eff}$. Eq. (34) can be simplified by assuming the slow varying amplitude approximation (Eq. (13)) which allow us to neglect the first term, now if we integrate the expression from 0 to L (length of the crystal) and considering that $I_i = 2cn_i\varepsilon_0|A_i|^2$ the solution in terms of the intensity is given by:

$$I_3 = \frac{8d_{eff}^2\omega_3^2I_1I_2}{n_1n_2n_3\varepsilon_0c^3}L^2sinc^2\left(\frac{\Delta kL}{2}\right), \tag{35}$$

here $\Delta k = k_1 + k_2 - k_3$ and it is called phase matching parameter.

SPDC is the reverse process of Sum-Frequency Generation (SFG) which is non-degenerate SPDC, i.e. different wavelengths for the two output photons. In classical non-linear optics this process is known as Parametrical Amplification in which the conservation of the energy requires that for every photon that is created at the difference $\omega_3 = \omega_1 - \omega_2$, a photon at the higher input frequency (ω_1) must be destroyed and a photon at the lower input frequency (ω_2) must be created. Thus, the lower frequency input field is amplified by process of difference-frequency generation (see Figure 2.3).

In the same way we calculated Eq. (34) we can derive the same type of equations for Parametric Amplification process (that lead to the Manley-Rowe relations [34]) for the case $\Delta k = 0$. Then, we get:

$$A_2(z) = i\sqrt{\frac{\omega_2n_1}{\omega_1n_2}}\frac{A_3}{|A_3|}A_1^*(0)\sinh(\alpha z), \tag{36}$$

$$A_1(z) = A_1(0)\cosh(\alpha z), \tag{37}$$

$$\alpha = \sqrt{\frac{\omega_2n_1}{\omega_1n_2}}\frac{\chi_{eff}^{(2)}|A_3|}{c}. \tag{38}$$

From these solutions we note that if there is not initial incident power at frequency ω_1 ($A_1(0) = 0$) the signal and idler photons would not exist and SPDC would not be possible. SPDC, as stated in its name, is the result of a spontaneous process since no other field stimulates the transition, except the vacuum fluctuations. For this reason the classical non-linear optics doesn't allow us to describe SPDC, a quantum description is needed. We can treat SPDC as the quantum evolution of a closed system (i.e. the electromagnetic field), where the Hamiltonian describing the nonlinear interaction determines the state of the field.

2.4.3 Quantum description

In order to derive an expression for SPDC state, we consider that a strong pump laser propagates along the principal axis of a non-linear crystal of length *L*, in our case we use the z-axis. (Figure 2.6). Assuming that the wave-vector distribution of the pump, signal and idler are mainly around this axis we can separate them into a longitudinal ($k^z \boldsymbol{e}_z$) and transversal $\boldsymbol{q} = (q_x e_x + q_y e_y)$, then the $\boldsymbol{k}$ vector is given by:

$$\boldsymbol{k} = k_j^z(\omega, \boldsymbol{q}) e_z + \boldsymbol{q}, \tag{39}$$

being ω the angular frequency and the index $j = p, s, i$ represents the pump, signal, and idler respectively.

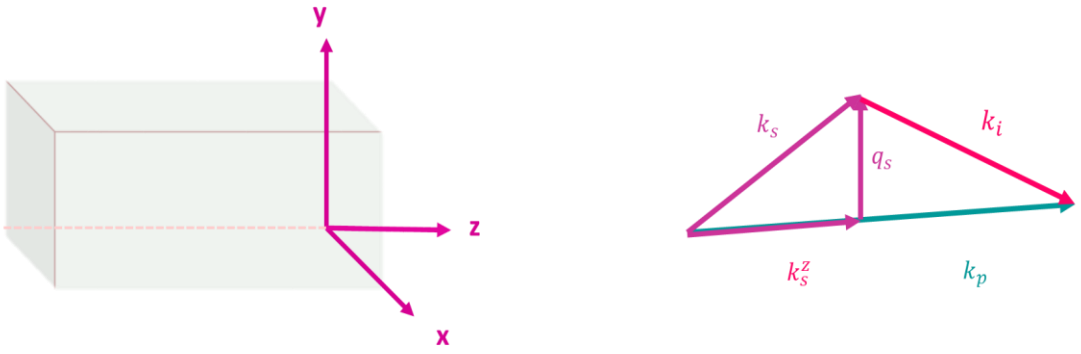

Figure 2.6 Coordinate system used as reference for the SPDC mode function.

The quantization of the electromagnetic field leads to a quantization of the second order polarization, so we can express Eq. (31) as:

$$\hat{P}^{(2)} = \epsilon_0 \chi^{(2)} \left(\hat{E}^{(+)} + \hat{E}^{(-)}\right)\left(\hat{E}^{(+)} + \hat{E}^{(-)}\right), \tag{40}$$

where $\hat{E}^{(+)}$ and $\hat{E}^{(-)}$ are the positive and the negative frequencies of the electromagnetic field operators [35]. It is possible to express $\hat{E}^{(-)}$ as function of the creation operator $\hat{a}^{\dagger}(\boldsymbol{k})$ at a position $\boldsymbol{r}_{\perp} = (x, y)$ and time *t* as:

$$\hat{E}_j^{(-)}(\boldsymbol{r}_{\perp}, t, z) = \sum_{k=H,V} \frac{\boldsymbol{e}_{k,j}}{(2\pi)^{3/2}} \int d\omega_j d\boldsymbol{q}_j \hat{a}_{k,j}^{\dagger}(\omega_j, \boldsymbol{q}_j) f(\omega_j^0) \times exp\big(ik_j^z(\omega_j, \boldsymbol{q}_j)z + i\boldsymbol{q}_j \cdot \boldsymbol{r}_{\perp} - i\omega_j t\big), \tag{41}$$

being $f(\omega_j^0) = \left(\hbar\omega/2\epsilon_0 c n_j(\omega_j)\right)^{1/2}$ a normalization factor. The positive frequency part of the field is the Hermitian conjugate of the negative one, such that $\hat{E}^{(+)}(\boldsymbol{r}_{\perp}, t, z) = \left(\hat{E}^{(-)}(\boldsymbol{r}_{\perp}, t, z)\right)^{\dagger}$. In Eq. (41) the operator $\hat{a}_{k,j}^{\dagger}(\omega_j, \boldsymbol{q}_j)$ creates a photon in the plane-wave spatial mode with transverse wave-vector $\boldsymbol{q}_j$, frequency ω_j, and polarization unit vector $\boldsymbol{e}_{k,j}$. On the other hand, the annihilation operator $\hat{a}_{k,p}(\omega_p, \boldsymbol{q}_p)$ removes a photon from the pump field. The creation and annihilation operators fulfill the commutator relations given in reference [35].

To calculate the state of SPDC after the interaction, we consider that the three-photon interaction is the initial state $|\psi_{initial}\rangle$ and begins at a time t_1 and finishes at a time t_2. Then we can describe the non-linear process with the time evolution operator as:

$$|\psi_{final}\rangle = exp\left(-\frac{i}{\hbar}\int_{t_1}^{t_2} \widehat{H}_I dt\right)|\psi_{initial}\rangle, \tag{42}$$

here $\widehat{H}_I$ is the Hamiltonian operator that mediates the SPDC interaction between the pump, signal, and idler fields that is defined as:

$$\widehat{H}_I = \epsilon_0 \int dV \chi^{(2)}(z) \hat{E}_p^{(+)}(\boldsymbol{r}_{\perp}, t, z) \hat{E}_s^{(-)}(\boldsymbol{r}_{\perp}, t, z) \hat{E}_i^{(-)}(\boldsymbol{r}_{\perp}, t, z) + H.c, \tag{43}$$

where the spatial dependence of the non-linear coefficient is $\chi^{(2)}(z) = \chi^{(2)} e^{\frac{i2\pi z}{\wedge}}$ with $\wedge$ the poling period along the crystal axis (z) and H.c stands for Hermitian conjugate.

From the first order perturbation theory [36], [37] (making a Taylor expansion of the exponential in Eq. (42) the interaction of an incident field $\hat{E}_p(\boldsymbol{r}_{\perp}, t, z)$ on a material of volume *V* with non-linear polarization $\hat{P}^{(2)}$, generates a state after the interaction at time t_2:

$$|\psi_{final}\rangle = \left(1 - \frac{i}{\hbar}\int_{t1}^{t2} \widehat{H}_I dt\right)|vac_s\rangle|vac_i\rangle + \cdots, \tag{44}$$

where $|\psi_{initial}\rangle = |vac_s\rangle|vac_i\rangle$. Here, we have just considered the first order contribution that corresponds to the vacuum state and the term related to the photon pair emission, the rest of the terms in the expansion correspond to the multiple pair emission. Nevertheless in the present thesis, we are mainly interested in the generation of pair photons. The remaining term (the two photon contribution) is proportional to the annihilation operator for the pump and the creation operator for the signal and idler photons, then we rewrite the term that contains $\widehat{H}_I$ in Eq. (44) as:

$$|\psi\rangle_{s,i}^{(2)} \sim \int d\boldsymbol{q}_s d\boldsymbol{q}_i \phi(\boldsymbol{q}_s, \omega_s, \boldsymbol{q}_i, \omega_i)\hat{a}^\dagger(\boldsymbol{q}_s, \omega_s)\hat{a}^\dagger(\boldsymbol{q}_i, \omega_i)|vac_s\rangle|vac_i\rangle, \tag{45}$$

where $|\psi\rangle_{s,i}^{(2)}$ is two photon contribution of Eq. (44). As a consequence of the low efficiency of the SPDC, it is possible to consider the pump as a classical field and the respective pair photons as quantum fields, we can express the term $\phi(\boldsymbol{q}_s, \omega_s, \boldsymbol{q}_i, \omega_i)$ know as the mode function in terms of the transverse momentum and frequency space as:

$$\begin{aligned}\phi(\boldsymbol{q}_s, \omega_s, \boldsymbol{q}_i, \omega_i) \\ &\propto \int dz d\boldsymbol{\rho} dt d\omega_p d\boldsymbol{q}_p E_p(q_p) S_p(\omega_p) \exp\left[-i(\omega_p - \omega_s - \omega_i)t\right] \\ &\times \exp\left[i\left(k_p^z(\boldsymbol{q}_p) - k_s^z(\boldsymbol{q}_s) - k_i^z(\boldsymbol{q}_i) - G^z\right)\mathrm{z}\right] \\ &\times \exp\left[\mathrm{i}(\boldsymbol{q}_p - \boldsymbol{q}_s - \boldsymbol{q}_i)\cdot\boldsymbol{\rho}\right].\end{aligned} \tag{46}$$

Eq. (46) contains all the information about the spatial mode ($E_p(q_p)$) and the spectral profile ($S_p(\omega_p)$) of the two-photon system, not only about their individual state but the correlations between them.

2.4.4 Approximation for the SPDC mode function

In order to solve the mode function is necessary to consider some approximations and assumptions. We assume a pump beam with a Gaussian temporal distribution, then the term $S_p(\omega_p)$ in Eq. (46) takes the form of:

$$S_p(\omega_p) = \exp\left[-\frac{T_0^2}{4}\,\omega_p^2\right], \tag{47}$$

being T_0 the pulse duration. In the case of a continuous wave (CW), T_0 tends to infinity. This thesis considers the frequency ω of each field as the sum of a constant central frequency ω^0 , and a small deviation from that frequency Ω, so that $\omega = \omega^0 + \Omega$.

For the spatial distribution of the pump, we assume an optical vortex with an amount $l_p\hbar$ of OAM per photon, so in this way we can project the pump beam in the Laguerre-Gaussian basis Eq. (21) and since the pump has a Gaussian distribution ($l_p = 0$) $E_p(q_p)$ simplifies to:

$$E_p(\boldsymbol{q}) = \sqrt{\frac{\omega_p}{2\pi}} \exp\left(-\frac{|\boldsymbol{q}|^2\, \omega_p^2}{4}\right), \tag{48}$$

Now for solving the integral over the time t we consider that the time is significantly longer than the time that light takes to travel the length of the non-linear crystal, but not so large that multiple photons are likely to be generated in a time t. In this case the limits of the integration can be extended from $-\infty < t < \infty$, then due to the energy conservation condition we get as a result:

$$\int_0^t dt\ \exp\left[-i(\omega_p - \omega_s - \omega_i)t\right] \rightarrow \int_{-\infty}^{\infty} dt\ \exp\left[-i(\omega_p - \omega_s - \omega_i)t\right] \propto\ \delta(\omega_p - \omega_s - \omega_i). \tag{49}$$

.

To integrate over the volume, we have to consider that the transversal dimensions of the crystal are much larger than in the region that the pump field is confined. The result of the integral leads to

$$\int_{-\infty}^{\infty} \mathrm{d}\boldsymbol{\rho}\, \exp[\mathrm{i}(\boldsymbol{q}_p - \boldsymbol{q}_s - \boldsymbol{q}_i)\cdot\boldsymbol{\rho}]\ \propto\ \delta(\boldsymbol{q}_p - \boldsymbol{q}_s - \boldsymbol{q}_i), \tag{50}$$

and

$$\int_{-L/2}^{L/2} \mathrm{d}z\, \exp\left[i\left(k_p^z(\boldsymbol{q}_p) - k_s^z(\boldsymbol{q}_s) - k_i^z(\boldsymbol{q}_i) - G^z\right)\cdot z\right] \propto\ sinc\left(\frac{\Delta k_z L}{2}\right). \tag{51}$$

Under this assumptions it is possible to rewrite Eq. (46) as:

$$\phi(\boldsymbol{q}_s, \omega_s, \boldsymbol{q}_i, \omega_i) = \mathrm{L}\sigma E_p(\boldsymbol{q}_s + \boldsymbol{q}_i) S_p(\omega_s + \omega_i) sinc\left(\frac{\Delta k_z L}{2}\right), \tag{52}$$

$\Delta k_z = (k_p(\boldsymbol{q}_s + \boldsymbol{q}_i) - k_s(\boldsymbol{q}_s) - k_i(\boldsymbol{q}_i) - \frac{2\pi}{\Lambda})$ represents the wave vector mismatch in the z axis for a periodically poled non-linear crystal with poling period Λ, ω_p is the pump waist at the center of the crystal. If we use the paraxial approximation around the point of perfect collinear quasi-phase matching (Δk_z) we get that $\Delta k_z = \frac{|\boldsymbol{q}_s - \boldsymbol{q}_i|^2}{2k_p^0} + \Omega_j \ldots + G_j(\boldsymbol{\Omega})$ where k_p^0 is the wave number at the central frequency, G_j is the group velocity and $\Omega_j = \omega_j - \omega_j^0$ the angular frequency deviation. Here we have restricted the considerations to the case of single-frequency continuous wave (CW) pump where $\Omega_s = \Omega_i \equiv \Omega$. Then we can express the bi-photon function Eq. (48) in terms of $(\boldsymbol{q}_s, \boldsymbol{q}_i, \Omega)$ as:

$$\Phi(\boldsymbol{q}_s, \boldsymbol{q}_i, \Omega) = \frac{L\,\tilde{\sigma}\omega_p}{\sqrt{2\pi}} \exp\left(-\frac{|\boldsymbol{q}_s + \boldsymbol{q}_i|^2\,\omega_p^2}{4}\right) \mathrm{sinc}\left(\frac{|\boldsymbol{q}_s - \boldsymbol{q}_i|^2\,L}{4k_p^0} - \frac{D\Omega L}{2}\right), \tag{53}$$

with D the inverse group velocity of the mismatch and $\tilde{\sigma}$ a dimensionless non-linear coefficient $\tilde{\sigma} = \sigma\sqrt{F_p}$ given by:

$$\tilde{\sigma} = \chi^{(2)} \sqrt{\frac{\hbar\,\omega_p\,\omega_s\,\omega_i\,F_p}{32\pi^2\epsilon_0 c^3 n_p n_s n_i}}, \tag{54}$$

here F_p represents the total flux (photons/s) of pump photons that traverse the non-linear crystal. For the next calculations we set that $F_p = 1$, such all probabilities are per-pump-photon probabilities.

We can see from Eq. (53) that the bi-photon mode function is formed by the contribution of the pump field, which determines the total transverse momentum and the energy storage for the process, and the phase matching contribution which as we described in section 2.4.1 ensures that the phase between the interacting fields is maintained along the propagation axis.

3 Theoretical results

In this section we study the general theory for SPDC in bulk periodically poled nonlinear crystal with emission in the visible spectral range. Here, we are particularly interested in some properties of the collected biphoton state, such as, the joint spectral density, the two- and single-photon collection probability, and the heralding ratio (pair/single photon collection ratio). These properties are calculated analytically and numerically as functions of experimental parameters, and compared with previous studies that have adopted similar scenarios.

3.1 Definition

3.1.1 Phase matching function

In an analogous way to the decomposition of an electromagnetic field as a series of plane waves, it is possible to decompose the field in other basis. The photon pairs generated during the SPDC process are distributed over a number of spatial modes and they are entangled in OAM due to the conservation laws of angular momentum. For instance, we can decompose a quantum state as a sum of Laguerre-Gaussian modes which are especially convenient since these modes are eigenstates of the OAM operator [29]. The state of a single photon in a LG mode is given by:

$$|l,p\rangle = \int d\boldsymbol{q} LG_p^l(\boldsymbol{q})\, \hat{a}^\dagger(\boldsymbol{q})|0\rangle, \tag{55}$$

where p represents the number of radial zero crossings and l the helical structure phase front around the singularity, and determines the OAM carried per photon in $\hbar$ units; the LG_p^l modes are given by Eq. (21). In this basis, we can express the SPDC mode function given by Eq. (45) as:

$$|\psi\rangle_{s,i}^{(2)} = \sum_{p_s p_i}^{l_s,l_i,} \int d\Omega\; C_{p_s p_i}^{l_s,l_i,}(\Omega)|l_s,p_s\rangle\,|l_i,p_i\rangle|\Omega_s\rangle|-\Omega_i\rangle. \tag{56}$$

As we mentioned in section 2.4, when OAM is conserved (as in the case of collinear SPDC) the pump beam transfers the total OAM to the photon pair according to $l_p = l_s + l_i$. In our case, we have assumed that the pump beam is of a Gaussian shape, thus $l_p = 0$ and

we can calculate the mode amplitude by projecting the bi-photon SPDC state Eq. (53) onto the target modes (Eq. (56)):

$$C_{p_s p_i}^{l_s, l_i,}(\Omega) = \left\langle l_s, p_s, l_i, p_i \middle| \psi_{SPDC}^{(2)} \right\rangle, \tag{57}$$

or

$$C_{p_s p_i}^{l_s, l_i,}(\Omega) = \int d\boldsymbol{q}_s d\boldsymbol{q}_i \Phi(\boldsymbol{q}_s, \boldsymbol{q}_i, \Omega) \left[LG_{ps}^{ls}(\boldsymbol{q}_s)\right]^* \left[LG_{pi}^{li}(\boldsymbol{q}_i)\right]^*. \tag{58}$$

The coincidence probability of finding a photon pair in a particular LG mode is giving by the square of Eq. (58).

3.1.2 Pair collection

As we will explain in further ahead to find the maximum achievable coupling efficiencies with respect to the focusing condition of the pump, as well as, the collection modes, it is convenient to express this focusing in terms of a dimensionless representation of focusing geometry, defined as:

$$\xi_j = \frac{L}{2\, z_j}, \tag{59}$$

where z_j is the Rayleigh range giving by $z_j = \frac{\omega_j^2 k_j}{2}$ and the index $j = p, s, i$ represents the pump, signal, and idler respectively. For a weak focusing strength $\xi \ll 1$, while for strong focusing $\xi > 1$.

Pair collection probability is the probability per pump photons that a pair is generated in the crystal, and that both photons of an entangled pair are coupled into their respective single mode fibers. The pair collection probability is usually given in terms of the focusing parameters:

$$P^{(2)}(\xi_p, \xi_s, \xi_i). \tag{60}$$

3.1.3 Single photon collection

The probability per-pump-photon of collecting a photon in the desired spatial mode, irrespective of the collection of the partner can be represented as:

$$P_s^{(1)}(\xi_p, \xi_s, \xi_i), \text{ and} \tag{61}$$

$$P_i^{(1)}(\xi_p, \xi_s, \xi_i) \tag{62}$$

where $P_s^{(1)}$ corresponds to probability for the signal photon and $P_i^{(1)}$ for the idler photon. Single-coupling efficiency is useful when maximizing the individual rate of photons present in the fibers.

3.1.4 Heralding

Heralding can be defined as the probability with which the presence of the signal photon heralds to the detection of the idler photon in its conjugate spatial mode. According to the Bayes' theorem we can write the heralding as:

$$\eta_s(\xi_p, \xi_s, \xi_i) = \frac{P^{(2)}(\xi_p, \xi_s, \xi_i)}{P_s^{(1)}(\xi_p, \xi_s, \xi_i)}, \tag{63}$$

$$\eta_i(\xi_p, \xi_s, \xi_i) = \frac{P^{(2)}(\xi_p, \xi_s, \xi_i)}{P_i^{(1)}(\xi_p, \xi_s, \xi_i)}. \tag{64}$$

3.1.5 Total pair and single photon collection probability

For calculating these probabilities, we will make use of the two photon ($S^{(2)}(\Omega)$) and single photon ($S^{(1)}(\Omega)$) spectral brightness which are described in detail in the next section. Additional to this, we should consider spectral filter functions of signal $\mathcal{H}_s(\Omega)$ and idler photons $\mathcal{H}_i(\Omega)$, thus the total pair-photon and single-photon collection probability in the presence of varied degrees of spectral filtering are defined as [38]:

$$P^{(2)} = \int d\Omega \mathcal{H}_s(\Omega)\mathcal{H}_i(-\Omega)S^{(2)}(\Omega), \tag{65}$$

$$P_s^{(1)} = \int d\Omega \mathcal{H}_s(\Omega)S^{(1)}(\Omega), \text{ and} \tag{66}$$

$$P_i^{(1)} = \int d\Omega \mathcal{H}_i(\Omega)S^{(1)}(\Omega). \tag{67}$$

where $P^{(2)}$ represents the pair-photon collection probability and the single-photon collection probability for the signal and idler is given by $P_s^{(1)}$ and $P_i^{(1)}$ respectively.

3.2 Theoretical model

The parameters considered for this section are based on typical bulk SPDC sources, which may be defined to have the following characteristics: the length of the medium is $L \geq$

$10\ mm$, its refractive index is $n \geq 1.5$; and emission spectral range, with $\lambda_p = 405\ nm$ and $\lambda_{s,i} = 2\lambda_p$. We will also consider degenerate type II collinear SPDC.

3.2.1 Spectral Bandwidth

For the spectral bandwidth in which the detected photons are distributed is necessarily to consider both the spectral bandwidth when both photons are collected, which is named two-photon spectral bandwidth $(\Delta\Omega)^{(2)}$ and single-photon spectral brightness $(\Delta\Omega)^{(1)}$ that it is given by the spectrum of all the photons detected, irrespective the of the photon partner detection. In certain SPDC experiments, when a pair of identical photons is preferable to a pair of highly correlated photons, one can narrowly filter the frequency spectrum of the signal and idler photons. The bandwidth of these frequency filters may be some orders of magnitude narrower than the natural bandwidth of the down-converted spectrum ($\Delta\Omega_F \ll \Delta\Omega_{SPDC}$).

We consider the extreme case, in which a spatial filter with a narrow passband, centered around the collinearly phase-matched central wavelengths ($\Omega = 0$) limit the number of detected signal and idler photons. Narrowband spectral filtering can be necessary to ensure spectral indistinguishability. In this case, the spectral bandwidth of the detected signal is determined by a passband spectral filter ($\Delta\Omega_F$), then Eqs. (65) to (67) can be approximated to the pair and single collection efficiency, respectively as:

$$P^{(2)} \sim S^{(2)}(0)\Delta\Omega_F, \text{ and} \tag{68}$$

$$P^{(1)} \sim S^{(1)}(0)\Delta\Omega_F. \tag{69}$$

3.2.2 Spectral Brightness and Collection efficiency

Filtering is one of the most important aspects of photon-pair engineering. Spatial filtering and more specifically coupling the photon pairs to a single mode fiber, like an optical fiber, is the first requirement for long-distance communications. The coupling efficiency is then a crucial parameter, and in order to calculate this parameter we should first determine the Spectral brightness, two- and single photon density. First, we will derivate an analytical solution for $S^{(2)}(\Omega)$, defined as the probability density for collecting a pair of photons per Hz bandwidth per-pump-photon. This is obtained by projecting the SPDC mode function into the Gaussian modes $p_s = p_i = 0$ and $l_s = l_i = 0$, since the spatial mode that propagates trough a SFM is approximately the fundamental mode. As we mentioned before, the

coincidence probability of finding a photon pair in a particular LG mode is giving by the absolute square of Eq. (58). In this way $S^{(2)}(\Omega)$ will be given by:

$$S^{(2)}(\Omega) = \left|C_{0,0}^{0,0}(\Omega)\right|^2. \tag{70}$$

For the calculation of Eq. (70) we have assumed the photons signal and idler are projected into a common spatial mode ($\omega_s = \omega_i$). Additional to this, it is necessary to consider the change of variable $\boldsymbol{q}_+ = \boldsymbol{q}_s + \boldsymbol{q}_i$ and $\boldsymbol{q}_- = \boldsymbol{q}_s - \boldsymbol{q}_i$. In order to simplify the calculation, it is convenient to change to cylindrical coordinate system as $|\boldsymbol{q}_+|^2 \to {\rho_+}^2$ and $|\boldsymbol{q}_-|^2 \to {\rho_-}^2$. Integrating Eq. (70) over ρ_+ we obtain:

$$S^{(2)}(\Omega = 0) = \frac{2\pi L^2 \tilde{\sigma}^2 \omega_p^2 \omega_s^4}{\left(2\omega_p^2 + \omega_s^2\right)^2} \left| \int_0^\infty d\rho \exp\left(-\frac{|\rho|^2\, \omega_s^2}{4}\right) sinc\left(\frac{|\rho|^2\, L}{4k_p^0}\right)\right|^2, \tag{71}$$

where we have changed to a cylindrical coordinates system such that $\rho = |\boldsymbol{q}_-|$. Here, we also have already considered the particular case when $\Omega = 0$. The exact solution of Eq. (71) is given by:

$$S^{(2)}(\Omega = 0) = \frac{8\pi\left(k_p^0\right)^2 \breve{\sigma}^2 \omega_p^2 \omega_s^4}{\left(2\omega_p^2 + \omega_s^2\right)^2} \left| tan^{-1}\left(\frac{2L}{k_p^0 \omega_s^2}\right)\right|^2. \tag{72}$$

For the narrowband limit, it is useful to normalize the collection probabilities with respect to the total number of photons emitted by the nonlinear crystal (total spectral brightness *F*) defined as:

$$F(\Omega = 0) = \int d\boldsymbol{q}_s d\boldsymbol{q}_i |\Phi(\boldsymbol{q}_s, \boldsymbol{q}_i, 0)|^2. \tag{73}$$

Substituting Eq.(53) in Eq. (73) and considering the same change of variable as before $\boldsymbol{q}_\pm = \boldsymbol{q}_s \pm \boldsymbol{q}_i$, the result of the total spectral brightness is:

$$F = \frac{k_p^0 \pi^2 \tilde{\sigma}^2 F_p\, L}{2} \tag{74}$$

Using Eq. (72) and Eq. (74) we can obtain the normalized two photon spectral brightness $S^{(2)}(0)/F(0)$. As we mentioned before, since we are considering narrowband filters, it is possible to approximate the two-photon spectral brightness to the pair collection efficiency according to Eq.(68). Then, the pair collection efficiency is found to be:

$$P^{(2)}(\Omega = 0) = \frac{16\, k_p^0 \tilde{\sigma}^2 \omega_p^2 \omega_s^4}{\pi L \left(2\omega_p^2 + \omega_s^2\right)^2} \left[\tan^{-1}\left(\frac{2L}{k_p^0 \omega_s^2}\right)\right]^2 \tag{75}$$

We would like to note that our result given by Eq.(75) is the same as the one reported in [1]. According to [22] and [39], a maximum collection efficiency is reached when:

$$\xi_p^{opt} = \xi_s^{opt}. \tag{76}$$

In order to obtain a relation between the beam waist of the pump and the collection modes, we substitute the definition of the focusing parameters, given in Eq. (59) in Eq.(76), so that:

$$\omega_s^{opt} = \sqrt{2}\, \omega_p^{opt}. \tag{77}$$

The above equation gives the conditions for the optimal parameters that must be satisfied in order to maximize the value of the collection efficiency. This result was also obtained by Palacios *et al.* [1]. If we substitute Eq.(77) in Eq. (75) this condition will lead to:

$$\frac{1}{2} tan^{-1}(\alpha) = \frac{\alpha}{1+\alpha^2}, \tag{78}$$

where $\alpha = {L}\Big/{k_p^0(\omega_p^{opt})^2}$. By solving numerically Eq. (78) we can determine that the value of α is a constant and equal to 1.39. In this way, we can clearly see that the values of ω_p^{opt} will depend on the parameter α as:

$$\omega_p^{opt} = \sqrt{\frac{L}{\alpha k_p^0}}. \tag{79}$$

Eq. (77) and Eq. (79) are then and as we expected, the optimal values that maximize the number of generated photons in the SPDC process. Figure 3.1 shows the pair collection probability defined in Eq. (75) for different crystal lengths, when the value of the pump waist is chosen to be $\omega_p = \omega_p^{opt}$. Three different values for the crystal length are plotted in the figure below, 10 mm (pink line), 15 mm (blue line), and 20 mm (green line). As we can observe, the maximum value we can reach in the three cases is $P^{(2)} \sim 82$ %, proving that the pair collection efficiency remains the same as a global maximum being independent of the value of L, as a consequence of approximating the field of the fiber's fundamental mode with a Gaussian function which is in agreement with the results reported on [1].

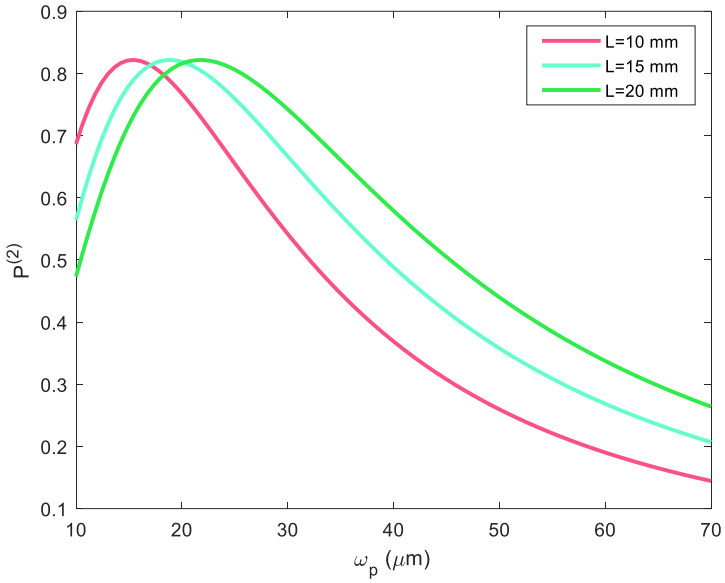

Figure 3.1 Pair collection efficiency ($P^{(2)}$) in term of the pump waist when is hold $\omega_p = \omega_p^{opt}$ for different crystal lengths.

We can express the pair collection efficiency (Eq. (75)) as function of the dimensionless focusing parameters ξ_p and ξ_s according to the definition given in Eq. (59). Figure 3.2 shows $P^{(2)}$ as function of ξ_p and ξ_s. In this figure, we have plotted $P^{(2)}$ for $L = 10\ mm$, since the behavior of the chart was not affected by changing the crystal length. Notice that there is an area (dark red) where is possible to get a coupling efficiency (pair collection) close to the maximum value, this what we call a regimen of good focusing. The fact that this regimen of a good focusing be broad, gives the advantage of having more options for choosing a set of parameters that lead us to a high efficiency and not being restricted to a single value as in Figure 3.1. This range for good focusing can be convenient for experimental work. We have a global maximum value for $P^{(2)}$ is reached when $\xi_p = \xi_{s,i} = 1.39$, which is compatible with the one reported on [2].

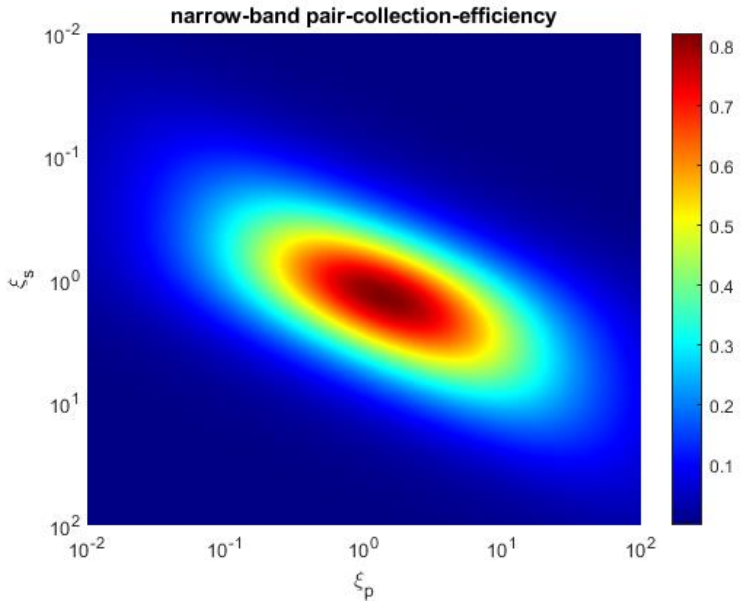

Figure 3.2 Pair collection efficiency $P^{(2)}$ as a function of the focusing parameters $\xi_{p,s,i}$ for the narrow band limit. The maximum value for the pair collection efficiency $P^{(2)} \sim 82$ % is reached when $\xi_p = \xi_{s,i} = 1.39$

In references [1], [22] it has been reported that the collection probabilities as well as, the heralding ratios are determined by the dimensionless ratios $\xi_p, \xi_{s,} \xi_{i,}$. We can notice that changing the crystal length has no effect on these parameters if the pump duration and confocal ranges are also scaled by the same factor. We can observe this behavior from Figure 3.1 and Figure 3.2. In the end, the crystal length just sets the bandwidth of the system.

Analogous to the definition of the two-photon spectral brightness, the single-photon spectral brightness ($S^{(1)}(\Omega)$) is the probability density for collecting a single-photon per HZ bandwidth, per-pump-photon. The calculation of $S^{(1)}(\Omega)$ is obtained by tracing out the partner photon's (in our case the photon idler) as:

$$S^{(1)}(\Omega_s) = \int d\boldsymbol{q}_i \left| \iint d\boldsymbol{q}_s \Phi(\boldsymbol{q}_s, \boldsymbol{q}_i, \Omega_s) \left[LG_{ps}^{ls}(\boldsymbol{q}_s) \right]^* \right|^2 . \tag{80}$$

Due to the complexity of the direct integration of Eq. (80) it is convenient to use the mode decomposition Eq. (57) that allows us to simplify the calculation, then we can rewrite the single-photon spectral brightness as:

$$S^{(1)}(\Omega_s) = \sum_{p_s=0}^{\infty} \left| C_{0,p_s}^{0,0,}\,(\Omega_s) \right|^2. \tag{81}$$

The fact that we can write the expression as a sum over p_s has its justification in the conservation of the orbital angular momentum in which for the Gaussian case it must be hold that $l_s = -l_i$, in such way, that if the idler photon is being collected in the fundamental mode $l_i = 0$, then the signal photon should be $l_s = 0$ and the higher order modes ($p_s \neq 0$) will be undetected.

For solving the integral given in Eq. (81), we have considered the same change of variables used for integrating Eq.(70), that is $\boldsymbol{q}_+ = \boldsymbol{q}_s + \boldsymbol{q}_i$ and $\boldsymbol{q}_- = \boldsymbol{q}_s - \boldsymbol{q}_i$. Where the transformation to the cylindrical coordinate system will be of the form $|\boldsymbol{q}_+|^2 \to {\rho_+}^2$ and $|\boldsymbol{q}_-|^2 \to {\rho_-}^2$. Taking into account these new variables (ρ_+ and ρ_-) we can rewrite the coordinate ${\rho_s}^2$ as:

$$\rho_s^2 = \frac{1}{4}[{\rho_+}^2 + {\rho_-}^2 + 2\rho_+\rho_- \cos(\varphi_+ - \varphi_-)]. \tag{82}$$

In this way, the new integral to solve becomes:

$$\begin{aligned} C_{0,p_s}^{0,0}(0) = {} & \frac{L\tilde{\sigma}\omega_p\omega_s^2}{8\pi L\sqrt{2\pi}} \int d\rho_+ d\rho_- d\varphi_+ d\varphi_- dz\; \rho_+\rho_- \exp\left(\frac{-\rho_+^2\omega_p^2}{4}\right) \\ & \times \exp\left(\frac{-\omega_s^2}{8}(\rho_+^2 + \rho_-^2)\right) \exp\left(\frac{iz\rho_-^2}{2k_p^0}\right) \sum_{k=0}^{p_s} (-1)^k \frac{p_s!}{(p_s-k)!\,k!^2} \\ & \times \left(\frac{\omega_s^2}{8}[{\rho_+}^2 + {\rho_-}^2 + 2\rho_+\rho_- \cos(\varphi_+ - \varphi_-)]\right)^k \end{aligned} \tag{83}$$

Note that in this last expression we have substituted the $sinc$ function for its exponential form. Using the binomial identity we can evaluate the integral in Eq. (83) over the radial variables and azimuthal angle ($\rho_+, \rho_-, \varphi_+, \varphi_-$) of the transverse component $\boldsymbol{q}$, we obtain the following expression for the single-photon spectral brightness:

$$
\begin{aligned}
&S^{(1)}(0) \\
&= \sum_{p_s=0}^{\infty} \left| f \sum_{k=0}^{p_s} \sum_{n'=0}^{k} \sum_{l=0}^{k-n'} 2^{n'} \, \frac{(-1)^k p_s!}{(p_s-k)!\,(k!)^2} \frac{k!\,d!}{(k-n')!\,n'!\,(d-l)!\,l!} \left(\frac{\omega_s^2}{8}\right)^k \right. \\
&\times \frac{\Gamma\left(\frac{2l+n'+2}{2}\right)}{2\left(\frac{\omega_p^2}{4}+\frac{\omega_s^2}{8}\right)^{[l+n'/2+1]}} \frac{2\left(1+(-1)^{n'}\right)\pi^{3/2}\Gamma\left(\frac{1+n'}{2}\right)}{\Gamma\left(1+\frac{n'}{2}\right)} \Gamma\left(\frac{2(d-l)+n'+2}{2}\right) \qquad (84) \\
&\left. \times \int_{-L/2}^{L/2} \frac{dz}{2\left(\frac{iz}{2k_p^0}+\frac{\omega_s^2}{8}\right)^{\left[d-l+\frac{n'}{2}+1\right]}} \right|^2,
\end{aligned}
$$

where $d = k - n'$ and $f = \frac{L\tilde{\sigma}\omega_p\omega_s^2}{8\pi\sqrt{2\pi}\,L}$. From this last expression we can clearly see that when we sum over the first value that corresponds to zero, i.e. $p_s = 0$ and $d - l + \frac{n'}{2} = 0$, Eq. (84) gives as result Eq. (72). On the other hand, when $\left(d - l + \frac{n'}{2}\right) > 0$, the analytical expression for all the values of p_s results in:

$$
\begin{aligned}
&S^{(1)}(0) \\
&= \sum_{p_s=0}^{\infty} \left| f \sum_{k=0}^{p_s} \sum_{n'=0}^{k} \sum_{l=0}^{k-n'} 2^{n'} \, \frac{(-1)^k p_s!}{(p_s-k)!\,(k!)^2} \frac{k!\,d!}{(k-n')!\,n'!\,(d-l)!\,l!} \left(\frac{\omega_s^2}{8}\right)^k \right. \\
&\times \frac{\Gamma\left(\frac{2l+n'+2}{2}\right)}{2\left(\frac{\omega_p^2}{4}+\frac{\omega_s^2}{8}\right)^{[l+n'/2+1]}} \frac{2\left(1+(-1)^{n'}\right)\pi^{3/2}\Gamma\left(\frac{1+n'}{2}\right)}{\Gamma\left(1+\frac{n'}{2}\right)} \Gamma\left(\frac{2(d-l)+n'+2}{2}\right) \qquad (85) \\
&\left. \times \frac{\left(\frac{iL}{4k_p^0}+\frac{\omega_s^2}{8}\right)^{-\left[(d-l)+\frac{n'}{2}\right]} - \left(-\frac{iL}{4k_p^0}+\frac{\omega_s^2}{8}\right)^{-\left[(d-l)+\frac{n'}{2}\right]}}{\frac{i}{2k_p^0}\left[(d-l)+\frac{n'}{2}\right]} \right|^2,
\end{aligned}
$$

In order to compare our results with previous ones, we select the value of $p_s = 2$, then the above equation reduce to:

$$
\begin{aligned}
&S^{(1)}(\Omega = 0) \\
&= 16\pi^4 \Bigg[\left| \frac{f k_p^0 \operatorname{acot}\left(\frac{k_p^0 \omega_s^2}{2L}\right)}{\frac{\omega_p^2}{4} + \frac{\omega_s^2}{8}} \right|^2 \\
&+ \left| \frac{f k_p^0}{\left(\frac{\omega_p^2}{4} + \frac{\omega_s^2}{8}\right)^2} \left(- \frac{\left(\frac{\omega_p^2 \omega_s^2}{8} + \frac{\omega_s^4}{16}\right) L k_p^0}{16\left(\frac{\omega_s^2}{8}\right)^2 {k_p^0}^2 + L^2} + \left(\frac{\omega_p^2}{4}\right) \operatorname{acot}\left(\frac{k_p^0 \omega_s^2}{2L}\right) \right) \right|^2 \\
&+ \left| \frac{f k_p^0}{\left(\frac{\omega_p^2}{4} + \frac{\omega_s^2}{8}\right)^3} \left(\frac{\left(\frac{\omega_p^2 \omega_s^2}{4} + \frac{\omega_s^4}{8}\right) L k_p^0 \left(-8 {k_p^0}^2 \left(\frac{\omega_s^2}{8}\right)^2 \left(\frac{\omega_p^2}{4} - \frac{\omega_s^2}{8}\right) + L^2 \left(-\frac{\omega_p^2}{4}\right) \right)}{\left(16\left(\frac{\omega_s^2}{8}\right)^2 {k_p^0}^2 + L^2\right)^2} \right. \right. \\
&\left. \left. + \left(\frac{\omega_p^2}{4}\right)^2 \operatorname{acot}\left(\frac{k_p^0 \omega_s^2}{2L}\right) \right) \right|^2 \Bigg]
\end{aligned}
\tag{86}
$$

As we already mentioned previously, but we wish to emphasize here, an analytical expression for the single-photon spectral brightness, to the best of our knowledge, has not been reported. Notice that the first term of Eq. (86) is the same expression that we got for the two-photon spectral brightness that corresponds to the case when $p_s = 0$.

Let us highlight the importance of having an analytical expression for $S^{(1)}$: We note that in the expression given in Eq.(83) there are at least for integrals that have to be performed, which for some of them the integration limits is infinity. This is not convenient from a numerical point of view, since these kind of calculations are time consuming and it also represents a high computing cost. On the other hand, having an analytical expression avoids these issues, and also allows us to see explicitly how each of the free parameters affect the behavior of the spectral brightness, and based on these observations we can find the optimal

conditions that maximize the value of single density. For $S^{(1)}$ we have also found a maximum value when $\xi_p = \xi_{s,i} = 1.39$. Figure 3.3 shows this probability assuming the condition given in Eq. (69). In the figure below, we can note that the shape of the plot is also not affected by changing L and the condition given by Eqs. (77) and (79) are hold for the single-photon probability, as well.

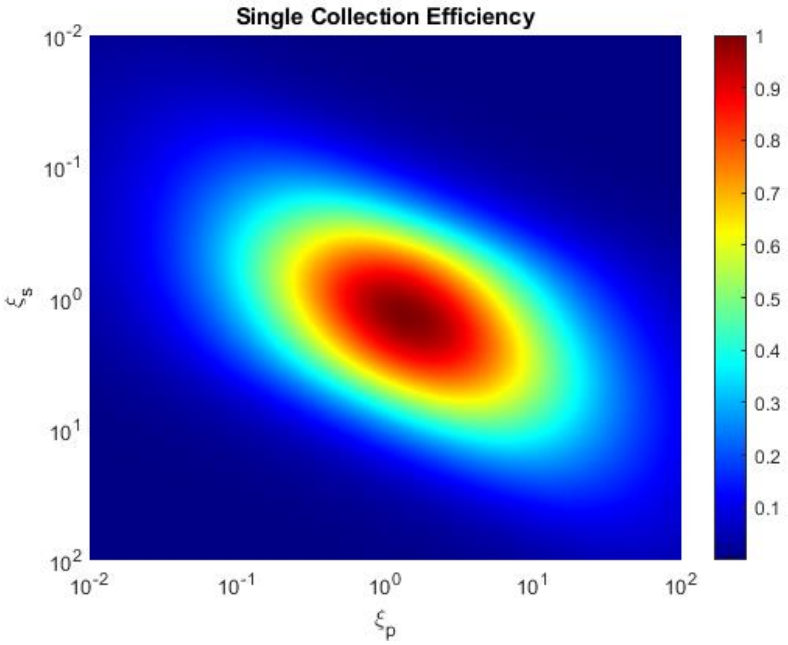

Figure 3.3. Single collection efficiency as a function of the focusing parameters for the narrow band limit, having a maximum when $\xi_p = \xi_{s,i} = 1.39$

Once that we have achieved both analytical solutions for the two- and single photon spectral brightness we can easily compute the next property of interest.

3.2.3 Heralding efficiency

Ideally, the detection of a signal photon is used to indicate the presence of an idler photon, although the photons are always emitted in pairs, conditions generally allow one photon to be emitted into a spatial mode, defined by the collection optics while its partner is emitted into a non-collected spatial mode. For this reason, it is desirable to have a high heralding ratio, which is defined as the probability of a single-photon state, conditional on a heralding detector signal, mathematically represented in Eqs.(63) and (64). Using narrowband filters, and the definitions of Eqs. (68) and (69), as well as the explicit expressions for the single- and two-photon spectral brightness, we can rewrite the heralding efficiency as:

$$\eta = \frac{S^{(2)}(\Omega = 0)}{S^{(1)}(\Omega = 0)} = \frac{\left|C_{0,0}^{0,0,}(0)\right|^2}{\sum_{p_s=0}^{\infty}\left|C_{0,p_s}^{0,0,}(0)\right|^2}. \tag{87}$$

We have found an analytical expression for $S^{(1)}$, which is valid for different values of p_s, however here we focus on the case $p_s = 3$ to compare the behavior of our heralding efficiency with the one reported in [2]. Then, using the results from Eqs. (75) and (85) we numerically calculated the heralding efficiency form Eq. (87). This is plotted in Figure 3.4, in terms of the focusing parameters. We would like to highlight that our figure shows the same behavior as the one obtained entirely numerical in [2] proving the veracity of our analytical expression in Eq. (85).

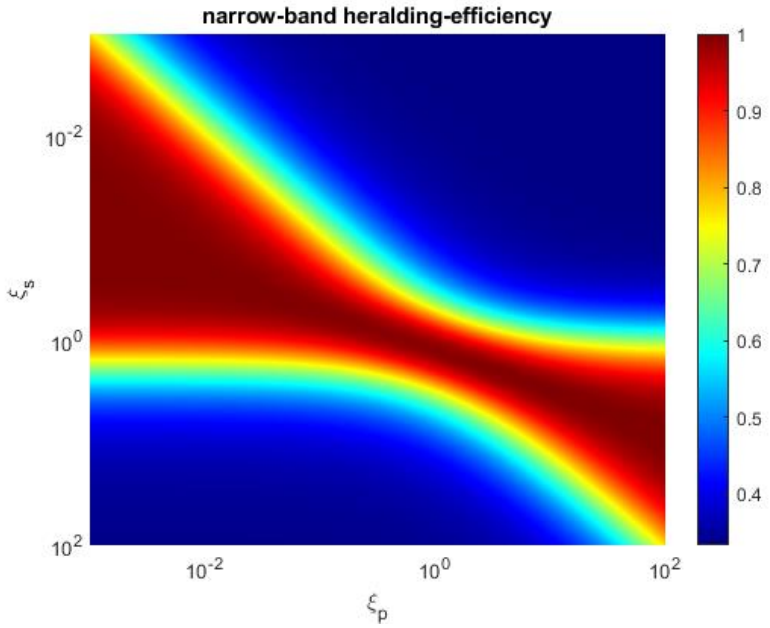

Figure 3.4 Heralding efficiency for the narrow band case when $\Omega = 0$ expressed in term of the confocal parameters.

As the probability of collecting both photons cannot exceed the probability of collecting one of the photons, the heralding ratio can be at most equal to 1. The most interesting characteristic observed in Figure 3.4 is that the heralding efficiency can reach values of η >99% for every value of ξ_p by choosing the correct confocal parameters $\xi_{s,i}$, offering a broader range for increasing the detection if we compared with the single value of the spectral brightness. On the other hand, previous studies [22], [23], [40] have demonstrated that

without the use of spectral filtering a trade-off between heralding efficiency and pair collection rates must be consider, i.e. η cannot be increased without decreasing $S^{(2)}$, and vice-versa; while the maximum of the pair rate is obtained for small values of the pump and collection waist, the heralding increase for large values of waist. However, in the limit of the narrowband, such as trade is not observed since a maximum heralding efficiency can be achieved for all the pump values. The veracity of these results was demonstrated experimentally in [18] where they have evaluated the improvement of the heralding efficiency by using large beam waist, as well as, spectral filtering showing that restricting the spectral bandwidth leads to a more beneficial trade-off, improving both quantities the heralding efficiency and the pair rate.

Finally, in Figure 3.5 the collection probability of finding a photon pair in a particular LG mode for SPDC $\left|C_{0,ps}^{0,0}(\Omega=0)\right|^2$ (that we can get from (85) without effecting the sum from p_s to ∞) is shown in terms of the focusing parameters of the collection modes $\xi_{s,i}$. for different fixed values of ξ_p. Each value of ξ_p corresponds to a different focused regimes: we have considered the values of $\xi_p = 0.01$ weakly focused, while $\xi_p = 1.5$ for a regime close to the optimal focusing; and finally $\xi_p = 5$ for strongly focusing. In the plot that corresponds to $p_s = 0$ for a fixed pump of $\xi_p = 1.5$, note that the highest peak is at $P^{(2)} \approx 0.82$ when $\xi_{s,i} \approx 1.5$ which agrees with the results from Figure 3.1 and Figure 3.2. In this figure we can clearly see how the collection efficiency decrease for higher order of p_s, finding in all the cases the higher fraction of emitted photon pairs into the fundamental mode. Note, however, that a heralding efficiency of $\eta > 99\%$ can be achieved, regardless of the choice of the pump mode, since mode contributions with $p \neq 0$ are suppressed by choosing a correct collection waist according to Figure 3.4.

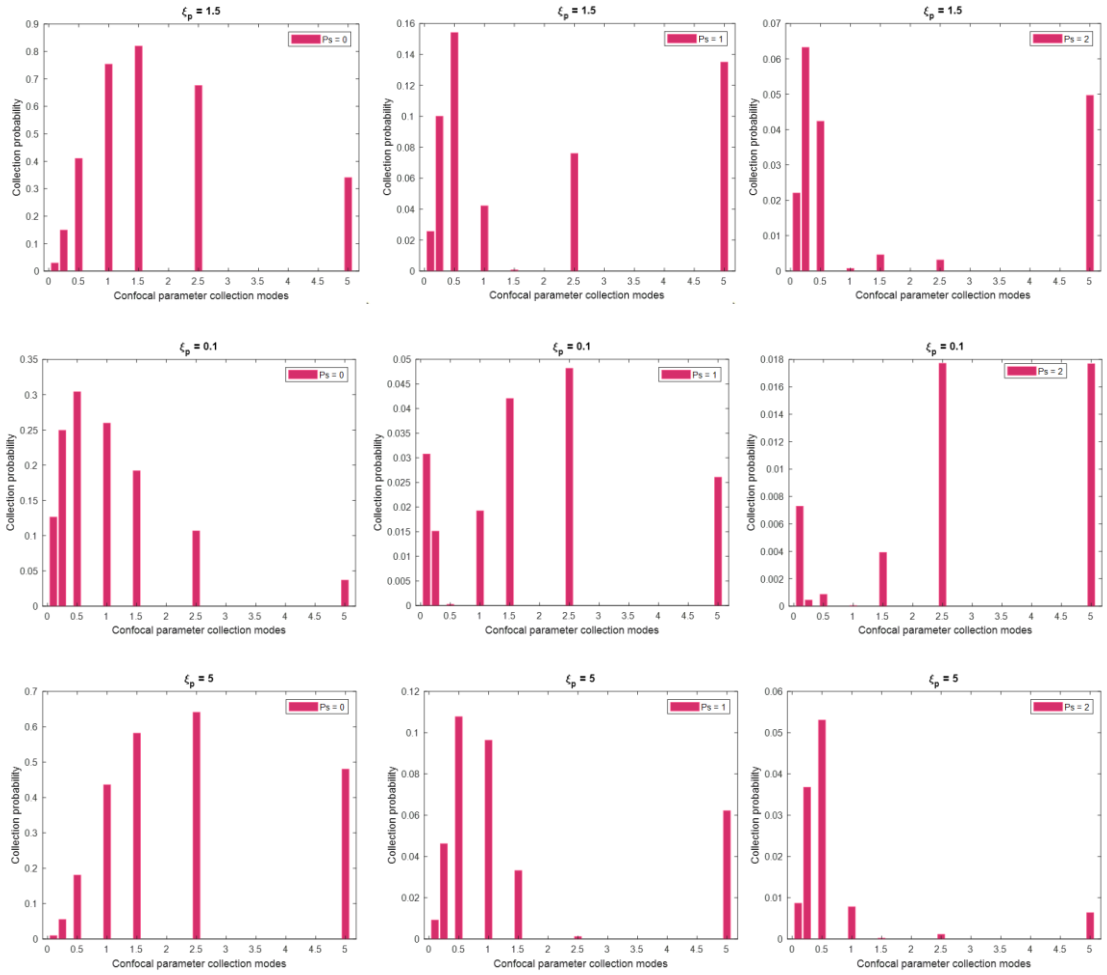

Figure 3.5. Coincidence probability of finding a photon pair in a particular LG mode $\left|C_{0,ps}^{0,0}(\Omega=0)\right|^2$ for SPDC in terms of the focusing parameters of the collection modes $\xi_{s,i}$. with a fixed ξ_p for: weakly focused ξ_p=.01, close the optimal focusing ξ_p=1.5; and strongly focusing ξ_p=5.

4 Conclusion

In this thesis we have investigated a two-photon state in space and frequency using a Gaussian pump beam, for SPDC bulk in non-linear crystals, considering a collinear geometry, and restricted to the spectral bandwidth to the narrowband case when $\Omega = 0$. We calculated analytic expressions for two- and single-photons spectral brightness. We have investigated the conditions and parameters such as the crystal length, size of the waist (for pump and collection modes) and the focusing parameters that maximize the pair- and single-collection efficiency. In the case of pair collection efficiency, our results are in agreement with the ones reported in [1]. On the other hand, an analytical expression for the single photon collection has not been (to the best of our knowledge) reported. We corroborated the veracity of our expression by calculating the heralding efficiency and comparing it with the one reported in [2].

In chapter 2, we have shown the essential factors contributing to the two-photon state in terms of space and frequency by deriving this expression from first principles. We began with deriving a general Hamiltonian for SPDC processes, and simplified it for the popular cases of bulk crystals.

In chapter 3, we have discussed how the single-photon and two-photon spectral brightness is affected by the choice of focusing parameters, and how this choice relates to heralding efficiency. For the two photons spectral density, we have confirmed that the optimal parameter that increase the pair collections ($P^{(2)} \approx 82\%$) is reached when $\omega_p^{opt} = \sqrt{\frac{L}{\alpha k_p^0}}$ and $\omega_s^{opt} = \sqrt{2}\,\omega_p^{opt}$ and independent of the crystal length, being in agreement with the results reported in [1]. We also have found that the value that maximized the Pair collection function expressed in terms of the confocal parameters is $\xi_p = \xi_{s,i} = 1.39$. Additional to this, we have calculated an analytical solution for the single photon spectral density that to the best of our knowledge has not been reported in previous works. We plotted how the pair collection efficiency varies when we focus the pump weakly, near to the optimal parameters and strongly finding (as it was expected) high efficiency for the values close to $\xi_p = 1.39$ and for the fundamental mode.

The results presented here, suggests that the presence of narrowband filters leads us to an improvement in both quantities (brightness and heralding efficiencies) for any values of the pump by choosing the correct confocal parameters. Understanding the behavior of these properties are of our interest for their application to experiments that develop bright sources with high heralding efficiency. Entangled photon sources with high heralding and brightness will be of particular significance to multi-photon experiments as well as for closing the detection loophole in fundamental experiments and device-independent QKD with entangled photons.

5 Appendix A: Methods for generation and manipulation of spatial modes

Since the experimental investigation of orbital angular momentum started in the ’90s, many approaches for creating and manipulating the spatial modes beams have been proposed and demonstrated. Until now, some of these attempts to design devices for generating such beams include spiral phase plates [9], computer-generated holograms imprinted onto spatial light modulators (SLMs) [41], [42], mode converters (array of cylindrical lenses) [43], q plates (non-uniform liquid crystal plates) [44], and some types of sorters [45], [46], Even though, these modes of light offer several advantages, the development of devices that allows us to manipulate and detect of spatial modes stills limited.

In this appendix we will describe some techniques and the experimental configuration for beam shaping light by the means of digital holography in the configuration of phase-only, complex amplitude modulation, a mode converter, as well as, the characterization of a commercial mode sorter (CAILabs PROTEUS-S-10-1550) based on the technique of Multiplane Light conversion (MPLC).

5.1 Light modulators and beam shaping

There are different techniques for generating Hermite-Gaussian and Laguerre-Gaussian beams being the liquid crystal on Silicon Spatial Light Modulators (SLM) [28] the most commonly used. A Spatial Light Modulator is a pixelated displays that can manipulate properties of light in which each pixel is an independent birefringent liquid crystal where the orientation of the optical axis of the liquid crystal is rotated by applying a certain voltage V (see Figure 5.1). The voltage is addressed by using the grayscale bitmap that is displayed on the SLM and depending on the orientation of the molecules the refractive index will change giving rise to a phase shift to the incoming beam with a specific polarization. The calibration of the SLM is done in such a way that a linear phase response to the incoming beam through the displayed grayscale image. Usually 8-bit are encoding, and allowing 256 colors, where black (0) corresponds to a phase equal to zero and white (255) corresponds to a 2π phase.

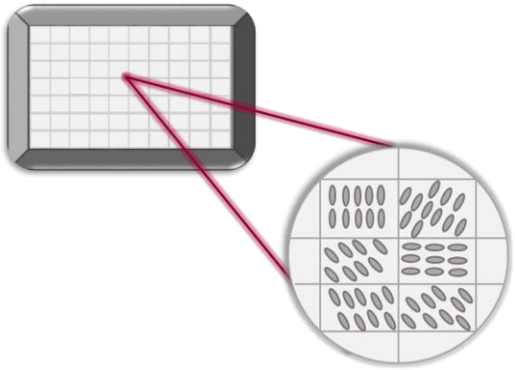

Figure 5.1 Schematic of a SLM screen, showing a different rotation of the optical axis in each pixel, therefore, a different phase modulation per pixel.

There are some difficulties that we should take into account when we use SLMs, among them it is the diffraction of the light in many directions due to the 2-D amplitude grating formed by each pixel and the space between them allows some rays of light to reflect without acquiring the desired phase (zeroth diffraction order) creating interfere with the diffracted light, which has the desired phase profile imprinted by the SLM, leading to a deterioration of the quality of the generated beams. To overcome this limitations, one can add a blazed grating to the generated hologram. The blazed grating has the advantage that a high percent of the light is diffracted into the desired order by moving the diffracted beam (first order) away from the undiffracted (zeroth order). Figure 5.2 shows some examples of the phase masks with blaze for generating HG and LG modes.

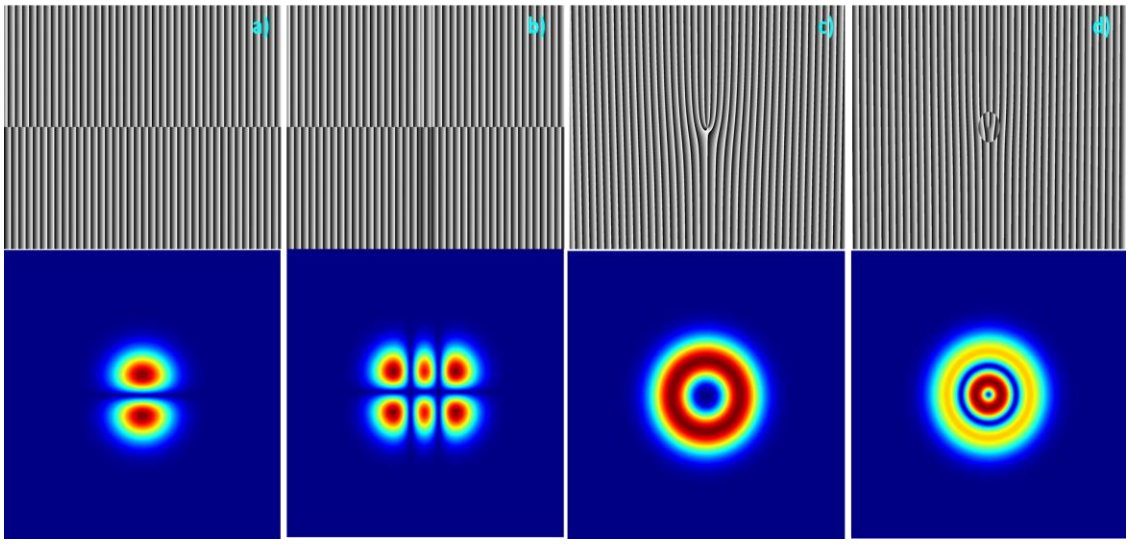

Figure 5.2 Phase modulation holograms for the generation of the HG and LG modes. In these case: a) HG01, b) HG21, c) LG30, and d) LG11.

Generating an arbitrary beam accurately requires phase and amplitude modulation simultaneously. Since most of the SLM are phase-only modulation, it is necessary to perform complex modulation (see Figure 5.3). This technique can be performed by making use of a modified hologram in which we can modulate the phase height of the grating programmed into the hologram [47]. The amplitude at any point in a plane can be controlled by adjusting the efficiency of the blazing in the corresponding region of the hologram. One can simply impose the desired intensity of the beam with some modifications to account for the mapping of phase height to diffraction efficiency to produce the hologram.

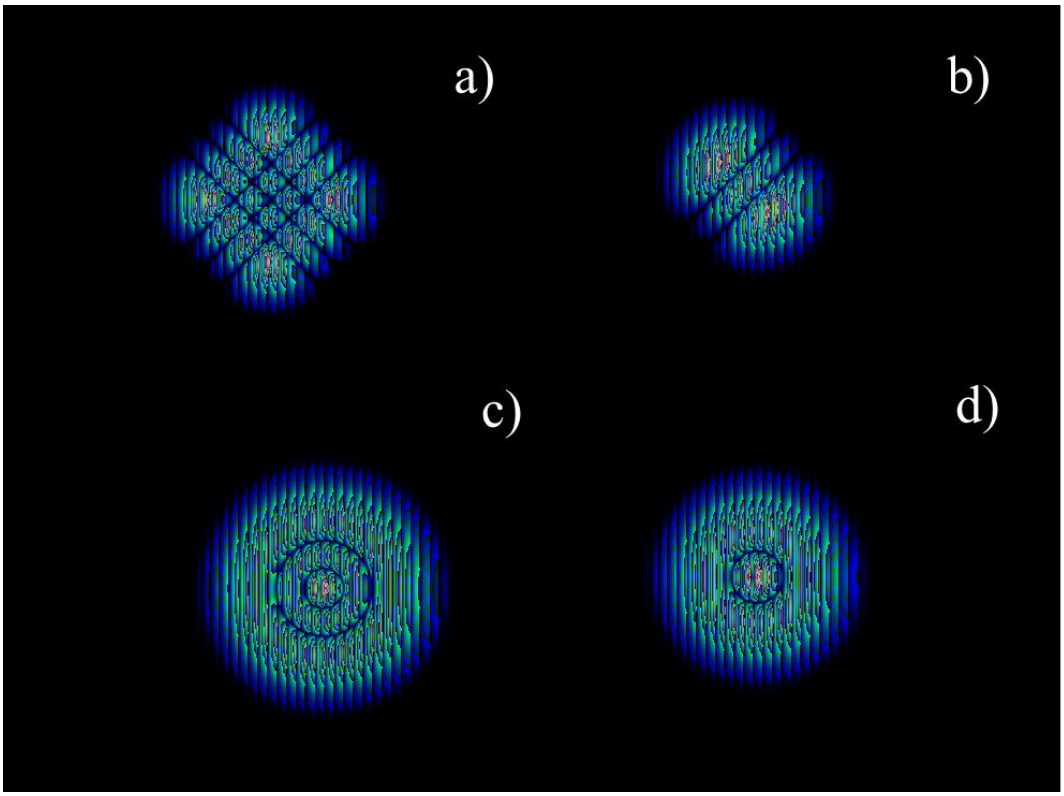

Figure 5.3 Complex amplitude modulation holograms for the generation of HG and LG modes. Where we have considered: a) HG11, b) HG30, c) LG01, and d) LG0-1.

Even though this generation method produces the spatial modes fairly accurately, it has some disadvantages. The input field is assumed to be a plane wave in its derivation [48], and even when this is a good approximation for the large Gaussian input beams, the intensity profile might not be optimally flat. Also, due to the amplitude masking, the method is very lossy.

5.1.1 Mode converter from HG to LG

As we mentioned in previous sections, LG and HG modes form a complete set of orthogonal functions, allowing us to express HG basis in terms of LG basis and vice versa. Based on the fact that HG modes oriented at 45° can be decomposed into a set of HG mode that can be rephrased and combine to form a particular LG mode by using an astigmatic mode converter (two cylindrical lenses) [43]. This HG modes can be expressed in terms of LG modes and vice versa through the relations:

$$LG_p^l(x,y,z) = \sum_{k=0}^{N} i^k b(l,p,k)\, HG_{N-k,k}(x,y,z) \tag{88}$$

where

$$b(l,p,k) = \frac{(N-k!\,k!)^{1/2}}{l!\,p!\,2^N} \frac{1}{k!} \frac{d^k}{dt^k} [(1-t)^l (1+t)^p]_t = 0 \tag{89}$$

From Eqs. (88) and (89) we can observe that the set of HG and LG modes are related to each other by:

$$l = n - m \tag{90}$$

$$p = \min(n,m) \tag{91}$$

Moreover, the correspondence between HG and LG modes is fixed by the mode order N, defined as:

$$N = n + m = 2p + |l| \tag{92}$$

From this last Eq. (92), it is possible to express the indexes of the HG modes in terms of the mode order N and the LG modes as:

$$n = \frac{N+l}{2} \tag{93}$$

$$m = \frac{N-l}{2} \tag{94}$$

Experimentally, all these relations can be used to generate LG modes starting from HG modes emitted by lasers, through mode converters using an arrangement of cylindrical lenses based on Eq. (88).

Transformation occurs due to the mode dependence of the Gouy phase obtained by the HG and LG modes. The cylindrical lens mode converters have two main forms: the $\frac{\pi}{2}$ converter which converts a HG to a LG mode or vice versa, and the π converter which exchanges the indices of the incoming mode and thereby converts a LG mode into one with opposite azimuthal dependence. When a beam is non-astigmatic, the Gouy phase is given by $(n+m+1)\varsigma(z)$, but for astigmatic beam the Gouy phase is characterized in terms of different Rayleigh planes $xz(Z_{Rx})$ and $yz(Z_{Ry})$ as:

$$\left(n+\frac{1}{2}\right)\arctan\left(\frac{z}{z_{Rx}}\right)+\left(m+\frac{1}{2}\right)\arctan\left(\frac{z}{z_{Ry}}\right) \tag{95}$$

A diagonal HG input beam that passes through two identical cylindrical placed at a distance of $\pm d$, induces a phase difference [43]:

$$\theta = 2\left[arctan\frac{1}{\beta}-arctan\beta\right], \qquad \beta=\sqrt{\frac{1-\frac{d}{f}}{1+\frac{d}{f}}} \tag{96}$$

The radius of curvature of both the components are equal to restore the beam back to the original shape (Figure 5.4). To achieve the required phase shift, it was found that the distance between the cylindrical lenses should be $d=\frac{f}{\sqrt{2}}$, with f being the focal lengths of the cylindrical lenses. To make the beam astigmatic only inside the cylindrical lenses, the mode matching condition has to be satisfied, which requires the input beam to have a Rayleigh range of $Z_{Rx}=f-d=(1-\frac{1}{\sqrt{2}})f$ and $Z_{Ry}=f+d=(1+\frac{1}{\sqrt{2}})f$. These conditions allow to implement experimentally the $\frac{\pi}{2}$-converter. For π-converter, it is possible to set $\theta=\pi$ leading to $d=f$ and as a result a collimated beam.

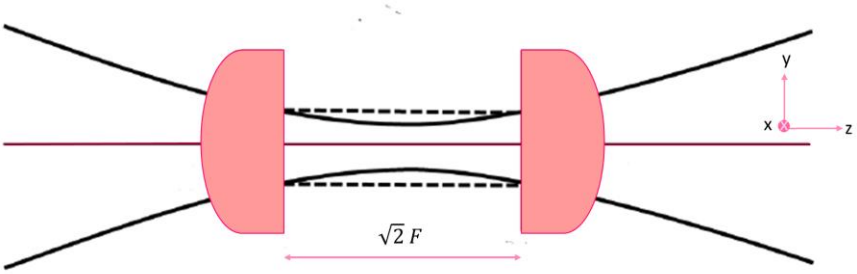

Figure 5.4 Sketch of a symmetric mode converter. The dashed curve denotes the Gaussian beam envelope in the (x,z) plane, and the solid curve in the (y,z) plane, with F is the focal length of the lenses. Here, L1 focuses the beam only along the y-direction, making the beam astigmatic and L2 restores the beam to the original shape or vice versa

The advantage of these lenses over holograms is that the optical efficiency of conversion is much higher, limited only by the quality of the antireflection coating of the lens.

5.1.2 Multiplane light conversion scheme

Although there are some well-known technique, such as "*phase flattening"*, where the incoming mode is allowed to pass through a hologram with its conjugate phase to produce a Gaussian mode which can be coupled to a single mode fiber [9]. This method is a projective measurement technique with an efficiency of $1/d$ being d the dimension of the system. Experimentally quantum communication would require a device that can map different spatial modes to specific points in space not only for one-dimension (typically the azimuthal l) but also that allows simultaneous sorting of both index p and l. This device is known as the mode sorter based on Multi-Plane Light Conversion technique.

Multiplane light conversion (MPLC) is a mode selective spatial multiplexing technique, which is performed by a unitary transformation on spatial modes, since it converts a given mode basis into another one, independent of the mode basis. Theoretically, for any desired set of N orthogonal spatial modes can be transform into any other set of N orthogonal modes through a sequence of transverse phase profiles, between the input and output plane, separated by free space propagation acting as a fractional Fourier transform operation. This succession of phase profile are usually generated by using SLMs or phase plates. Phase profiles can be calculated by an algorithm called "wavefront matching" which generates the phase masks at the different planes in the propagation direction by calculating the overlap of

the input field and the complex conjugate of the output field at all points in space for a specific plane (and for each plane). At each step the phase mask is updated to become the phase of the superposition of the overlap between each pair of the input field (A_n) and the output modes (B_n*) at a specific plane (n) where the updated mask is given by $\varphi_n = \arg\{\sum_{n=1}^{N} A_n B_n^*\}$, with N is the total number of modes and A_n and B_n* are the nth modes in the forward and backward direction.

The input field is multiplied by the calculated phase at that plane then propagated to the next one iteratively. The process is repeated until the last plane and then the same algorithm is used backward propagation (see Figure 5.5) then the iteration is repeated and continued until both fields (input and output) converge at each plane during the propagation forward and backward.

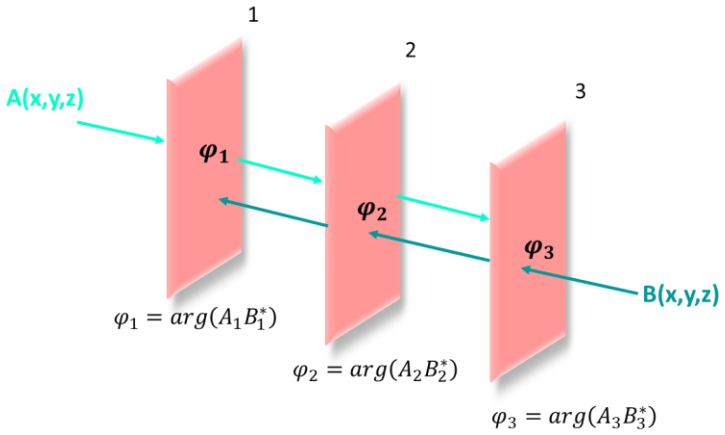

Figure 5.5 Sketch of the wave-front matching procedure. *A(x,y,z)* is the input field and *B(x,y,z)* the output field (and vice versa), calculating the overlap of these field at an specific plane n (in the figure n=1,2,3) and updating the phase mask $\varphi_n = \arg\{\sum_{n=1}^{N} A_n B_n^*\}$.

MPLC can be used in the reverse direction, performs the inverse unitary transform generating the same modes operating as a de-multiplexer. In practice, MPLC is implemented using a multi-pass cavity, which is formed by a mirror and a single reflective phase plate where the successive phase profiles are all produced. Nevertheless, the number of phase profiles required for a given MPLC is a trade-off between the number of modes, the complexity of the phase and amplitude profile of the modes [49].

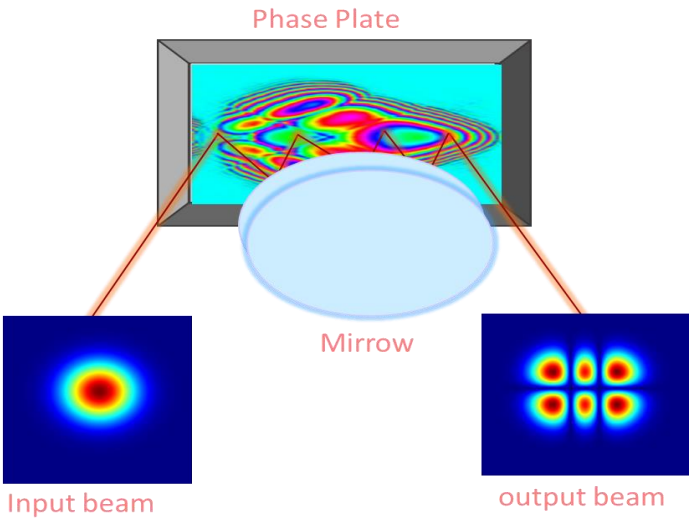

Figure 5.6 Schematic of the multiplane light conversion system [Depiction of the transformation of a Gaussian mode at the input to any other spatial mode (here HG11) and vice versa]

As we mention before MPLC is one of the most promising techniques since it can measure full transverse structure of the spatial modes with good efficiency. Recently, a Laguerre Gaussian mode sorter which can decompose 210 modes into a Cartesian grid of Gaussian spots was realized by using MLPC and requiring only seven plane [50]. In this article the MPLC was used to transform a triangular array of Gaussian spots to Hermite-Gauss modes which later are converted to Laguerre Gaussian modes using an array of cylindrical lens as a mode converter. The experimental scheme involved the beam propagating between an SLM and a mirror to perform the required transformation. The screen of the SLM is split into seven planes where each of the required phase mask is displayed and the free space propagation is obtained by the successive reflections from the mirror. Figure 5.6 shows a schematic MPLC based mode transformation where a Gaussian mode is transformed to a particular Hermite-Gaussian mode. MPLC is proposed to overcome several disadvantages of the already existing spatial mode transformations, specifically OAM detection schemes as it can perform true two-dimensional decomposition in any spatial mode basis. However, even though there are some spatial mode sorters of light which are commercially available [49], this sorting technique still at their early development stage.

5.2 Experiments

5.2.1 SLM's Gamma curve characterization

For these experiments we used a SLM-200 Santec which has a display of 1920*1200 pixels and a pixel pitch of 8 µm. The value of the phase is related to the value of the gray level read by the SLM, in this case 10 bits (1024-gray levels). However, even when this is linear, we had to characterize it due to some irregularities of the SLM for reading the holograms. For this configuration we required a quarter wave plate (QWP) with its fast axis at 45° with the horizontal, and a SLM placed parallel to the QWP with its extraordinary axis parallel to the horizontal one Figure 5.7. This characterization was performed for a wavelength $\lambda = 1550\ nm$.

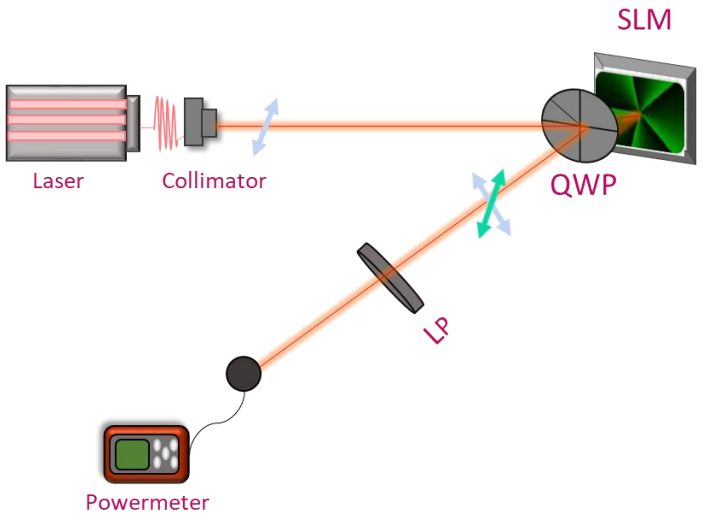

Figure 5.7 Set-up for the characterization of the Gamma curve

A beam propagating through this system impinging at normal incidence is going to see a QWP at 45°, a phase modulation (δ(x,y)) in the horizontal polarization component proportional to the $n_e(V) - n_o$, a reflection from the SLM, and finally, the same QWP but this time at 135°. Applying the Jones Matrix formalism, this system is described by [51]:

$$M = R\left(\frac{3\pi}{4}\right) J_{QWP} R\left(-\frac{3\pi}{4}\right) \begin{pmatrix} -1 & 0 \\ 0 & 1 \end{pmatrix} J_{SLM} R\left(\frac{\pi}{4}\right) J_{QWP} R\left(-\frac{\pi}{4}\right) \tag{97}$$

Solving Eq. (97) gives as a results

$$M = e^{i\delta(x,y)/2}\begin{pmatrix} -\sin\left(\frac{\delta(x,y)}{2}\right) & -cos\left(\frac{\delta(x,y)}{2}\right) \\ cos\left(\frac{\delta(x,y)}{2}\right) & -sin\left(\frac{\delta(x,y)}{2}\right) \end{pmatrix} \quad (98)$$

The Jones matrix is given in the terms of a rotation matrix with and extra phase term of $\frac{\pi}{2}+\frac{\delta(x,y)}{2}$ with respect to the horizontal. Experimentally we can get this phase factor by measuring the polarization at an angle ϕ.

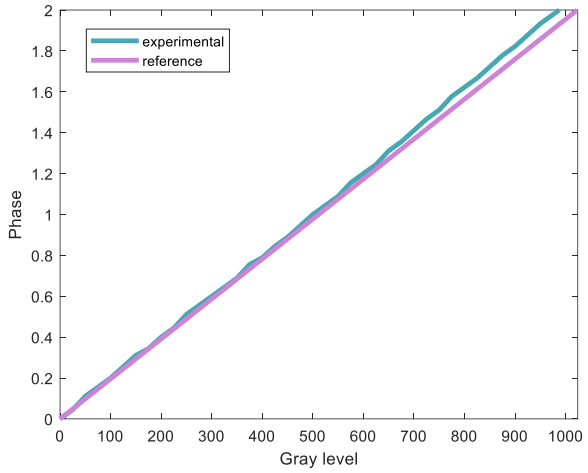

Figure 5.8 Gamma curve that represents the value of the phase in terms of the gray level. The purple line is used as a reference to show how a good calibration of the system should be. The blue line shows the experimental data obtained by using the method described above.

The use of this method is possible since the incidence angle on the SLM is small. The polarization rotation is found using a power-meter and a linear polarizer (LP), that is rotated θ radians, until we find a minimum intensity, which occurs when $\theta = \frac{\pi}{2}+\frac{\delta(x,y)}{2}-\frac{\pi}{2}$. Then, the phase is:

$$\delta(x,y) = 2\theta \quad (99)$$

The value of the phase is found for different values of gray level set in the SLM until completing a period (from 0 to 2π) as it shown in Figure 5.8.

5.2.2 SML configuration

For the generation of Hermite-Gauss and Laguerre-Gauss beams, the phase masks were displayed on a spatial light modulator (SLM-200 Santec), the reflectivity of the SLM used in

our experiments is about 93%. The diffraction efficiency is defined as the ratio of the power diffracted in the first order with the respective blaze level to the power in the zeroth order with non-addressed SLM.

For the configuration of phase only modulation of the incident field on the SLM, the far field diffraction will generate the desired field distribution (Figure 5.9). The modulated beam is obtained at the focal plane of a lens after the SLM, which is equivalent to propagate the beam to the far field or performing the Fourier transform. In the case of simultaneous phase and amplitude modulation scheme, the corresponding field is generated in the near field of the SLM which it is equivalent to allow selectively the desired field distribution be modulated in both phase and amplitude to propagate in a specific diffraction order (in our case the first order). Using a telescopic arrangement is used to detect the desired field at the image plane of the SLM, by placing a spatial filter at the focal plane of the first lens to spatially filter the unwanted diffraction orders (Figure 5.11).

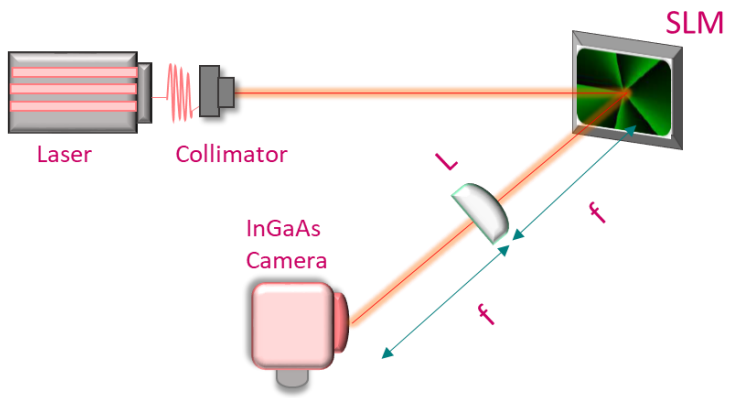

Figure 5.9 Add figure of phase only generation and the generated beams.

Phase only modulation does not provide beam profiles as it is desired due to the fact that the holograms do not account for exact amplitudes. This feature exhibits in the form of the spreading intensity in the lobes of the Hermite-Gauss beams in Figure 5.10. We could observe some inhomogeneity in the intensity of the lobes, related to the imperfect phase front of the beam incident on the SLM. Another possible reason could be inaccurate positioning of the beam profiler (Thorlabs BP209-IR/M) exactly at the Fourier plane of the lens.

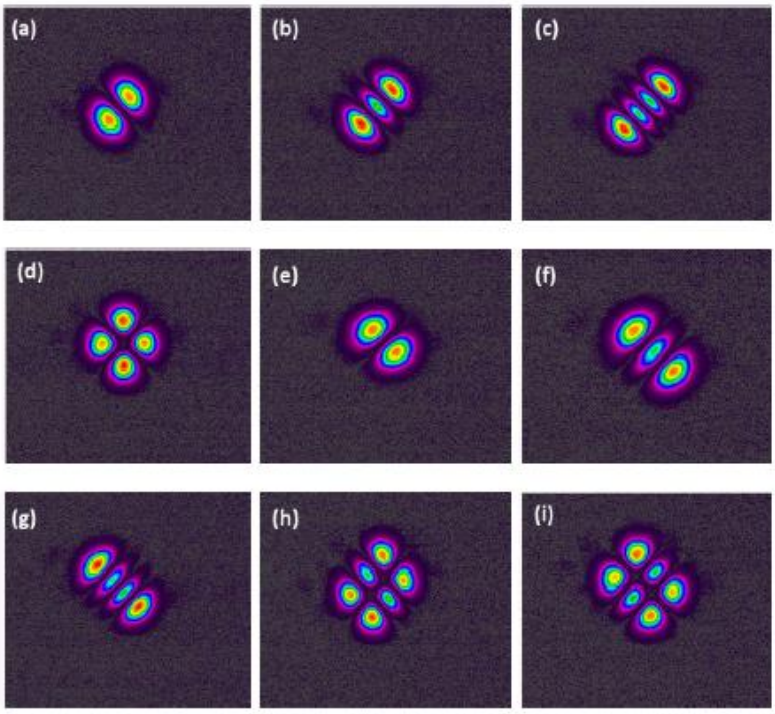

Figure 5.10 Intensity profiles in phase modulation only for: a) HG_{10}, b) HG_{20}, c) HG_{30}, d) HG_{11}, e) HG_{01}, f) HG_{02}, g) HG_{03}, h) HG_{21}, i) HG_{12}

To obtain the desired HG, LG modes more precisely, the incident field should be modulated in both phase and amplitude. Figure 5.12 shows the generated modes at the image plane of the SLM.

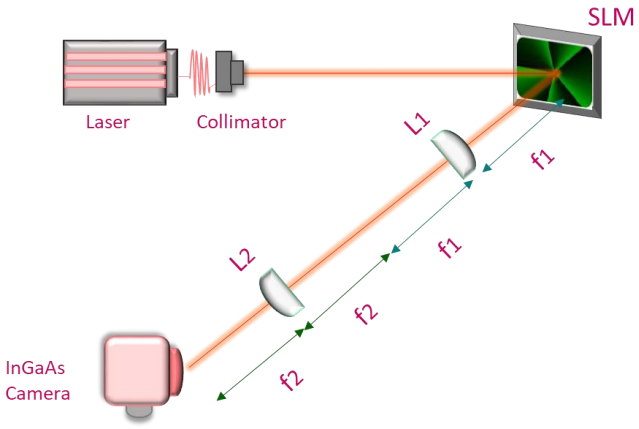

Figure 5.11 Add figure of complex amplitude modulation and the obtained beam.

The intensity profiles of the Hermite-Gauss modes using the amplitude modulation matches well with the expected intensity profiles. Figure 2.1 shows some of the other beams generated using amplitude modulation technique. Even though the intensity profile of the

generated beam matches well with the theoretical predictions, this technique is extremely lossy as we are allowing only the required intensity patterns from the input beam to diffract into the first order.

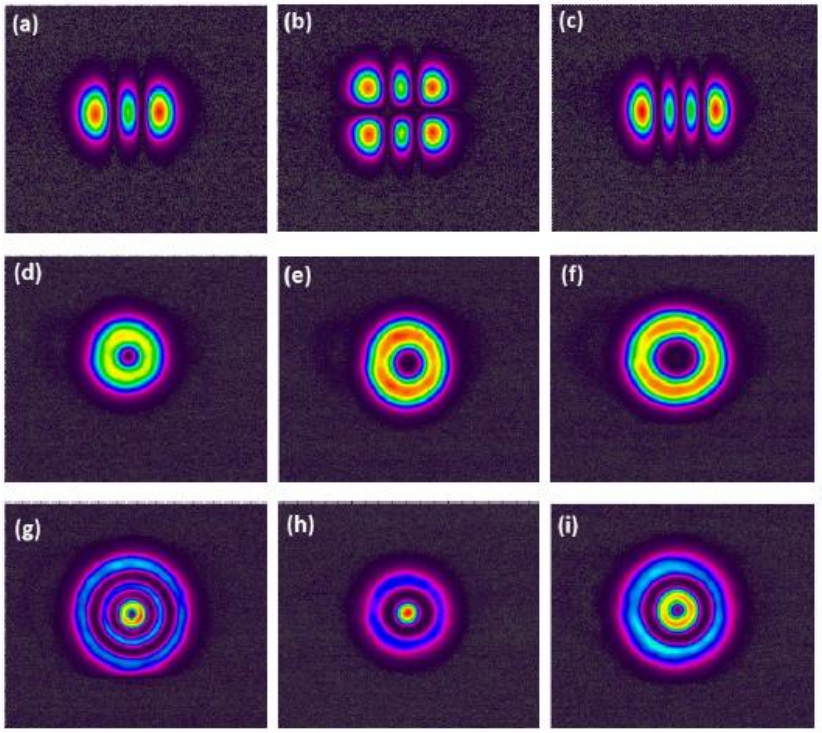

Figure 5.12 Intensity profiles in amplitude modulation for: a) HG_{20}, b)) HG_{21}, c) HG_{30}, d) LG_0^1, e) LG_0^2, f) LG_0^3, g) LG_1^2, h) LG_1^0, i) LG_1^1

5.2.3 Multiplexing scheme

The mode sorter (CAILabs PROTEUS-S-10-1550) works as a multiplexer by performing a transformation in the Gaussian spots at each spatial position into a corresponding Hermite-Gauss mode by MPLC. The CAILabs PROTEUS-S-10-1550 is designed to perform these transformations for the first 10 modes of the Hermite-Gauss mode family. In this device, the Gaussian spots are fiber coupled and can act as a spatial mode multiplexer if we couple into the single mode fibers simultaneously. The experimental configuration to characterize the transmission efficiency of each of the channel for multiplexing is shown in Figure 5.13. A collimated beam from a diode laser emitting at 1550 nm (QSDIL-500) is coupled to a single mode fiber, which is connected to each of the fiber ports of the mode sorter to measure the corresponding efficiency of the port, on the other side of the device (playing the role of the output) there is a multimode fiber and at a distance of approximately 3 mm the aspheric lens

was placed. In order to see the output of the sorter, we placed and InGaAs camera in front of the MMF.

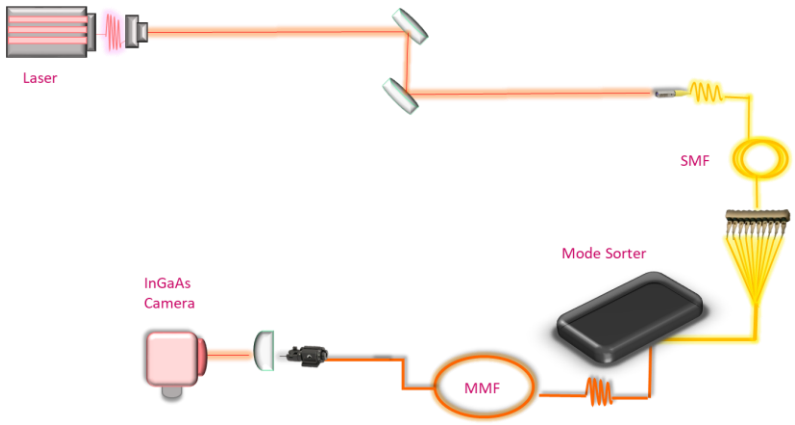

Figure 5.13 Experimental setup for multiplexing characterization.

During the characterization of this device we found that the intensity profiles of the modes where not matching, since when light propagates through a MMF experiences spatial distortions that scramble the intensity profile. We attributed this problem to the fact that when we excite a mode at the input, we are also exciting the "degenerated" modes of the optical fiber as it is explained in [52]. In our experiment, as we can see in Figure 5.14 when the HG03 mode propagates, we observe at the output the following modes: $HG_{03} + HG_{12} + HG_{21} + HG_{30}$ as a result of modes from the same group mixing inside the fiber provoked that input and output were different. This can happen in only a few meters but the distance in our experiments is small.

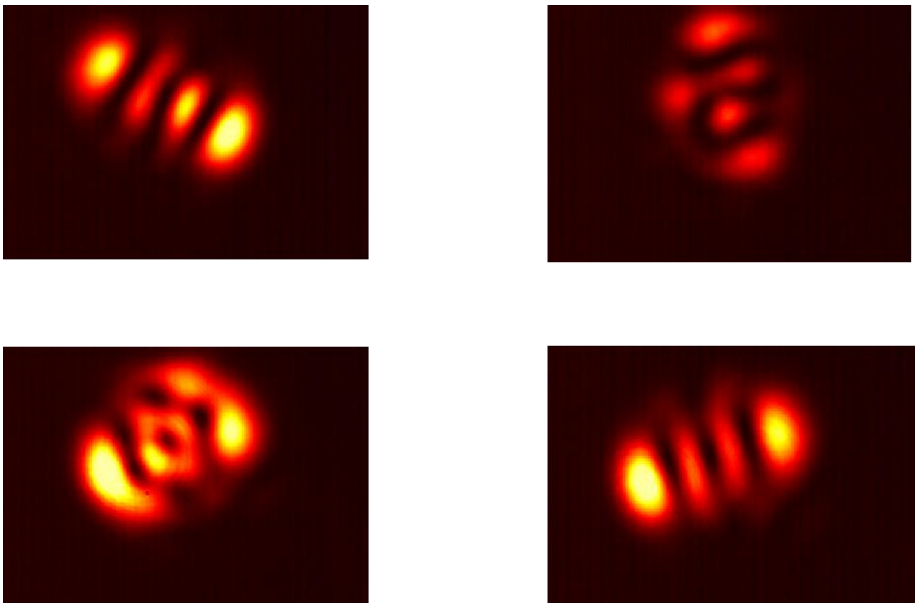

Figure 5.14 HG modes with the mixing modes problem.

As a solution to overcome this issue it is a free space output which will allow us the possibility to retrieve our input information because, without a fibered output we can delete this mixing phenomenon.

5.2.4 De-multiplexing scheme

The aim of the characterization of the device as a de-multiplexer was to understand how efficiently it can be decomposed arbitrary beam shapes in the Hermite-Gauss basis. For this, we generated HG beams and LG beams using a spatial light modulator as is show in Figure 5.15 experimental setup for the de-multiplexer characterization.

Since the SLM is polarization dependent, the collimated incident beam from a 1550 nm laser is split into orthogonal polarizations using the PBS and in this way the beam will only acquire the phase displayed on the screen of the SLM. We obtained a nearly Gaussian beam with an approximate beam diameter of 0.6 mm, which is then expanded to nearly 4 mm using the pair of lenses L1 (f=100 mm) and L2 (f=200 mm) before being incident on the SLM. The first order diffracted beam from the SLM is modulated in phase and amplitude and passes through the telescopic system consisting of L3 (f=100 mm) and L4 (200 mm). An iris aperture was placed at the focal plane of the lens L3 in order to eliminate the diffraction orders other than the first propagating through the system. After lens L4 was placed the InGaAs camera to make sure that our desire mode was generated properly. Lenses L3 and

L4 were chosen such way that the beam diameters of the Gaussian beams match at the image plane of the SLM. The lens L5 (f= 100 mm) was placed at a distance equal to its focal length from the image plane of the SLM, L5 was used to match the beam waist of the generated HG beams from the SLM with the mode sorter.

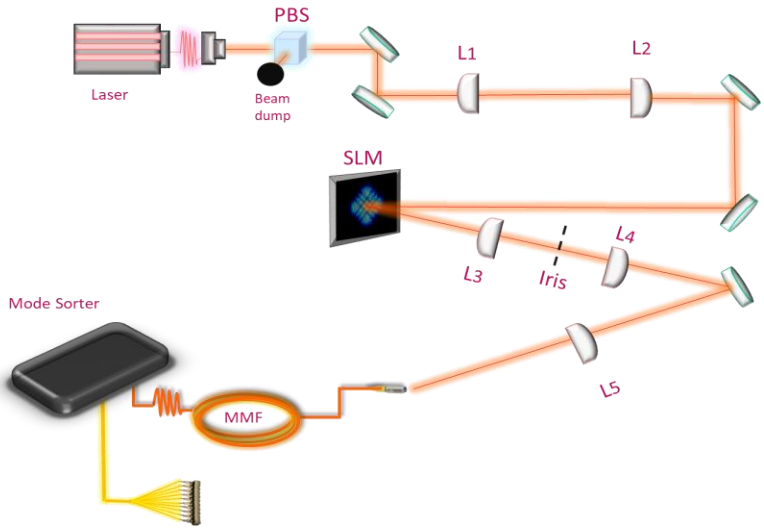

Figure 5.15 Experimental setup for de-multiplexing characterization.

It is possible to achieve the required beam parameters by making appropriate changes in the phase masks displayed on the SLM, in our case we have chosen a beam waist parameter of 1 mm for the beams which gets de-magnified after passing through the telescope in such a way that it can match with the beam from the sorter at the image plane of the SLM. Unfortunately, regarding to the same problem that we mentioned in the section above the propagation of the generated HG and LG beams through the device and the measurement of the coupling efficiency as well as cross talks between the channels was not possible to achieve.

5.3 Conclusions

In this work, we also have studied the sorting of spatial modes with the aim of using them in quantum optical experiments, specifically in analyzing the correlations between the photon pairs in their spatial modes. We selected a laser diode emitting at 1550 nm for the experiments, which is in the telecommunication spectral range. Nevertheless, we could not complete the characterization of the device due to the phenomenon of mode mixing inside the multimode fiber included in the sorter. Our next step would be the full characterization

of the sorter in free space to delete the effect and allows us to compare its efficiency compared with other methods with the aim of use the MPLC based mode sorter for generating modes with OAM that can be used for high dimensional QKD experiments for a wavelength of 1550 nm.

6 References

[1] S. Palacios, R. de J. León-Montiel, M. Hendrych, A. Valencia, and J. P. Torres, "Flux enhancement of photons entangled in orbital angular momentum," *Opt. Express*, vol. 19, no. 15, pp. 14108–14120, 2011, doi: 10.1364/oe.19.014108.

[2] F. Steinlechner, "Sources of Photonic Entanglement for Applications in Space," ICFO - Institut de Ciencies Fotoniques, 2015.

[3] M. A. Nielsen and I. L. Chuang, *Quantum Computation and Quantum Information*, !!0th Anniv. Cambridge, 2010.

[4] R. Loudon, *The Quantum Theory of Light*, 3rd ed. Oxford Science Publications, 2000.

[5] C. Schaeff, R. Polster, R. Lapkiewicz, R. Fickler, S. Ramelow, and A. Zeilinger, "Scalable fiber integrated source for higher-dimensional path-entangled photonic quNits," *Opt. Express*, vol. 20, no. 15, pp. 16145–16153, 2012, doi: 10.1364/oe.20.016145.

[6] I. Marcikic, H. de Riedmatten, W. Tittel, V. Scarani, H. Zbinden, and N. Gisin, "Time-bin entangled qubits for quantum communication created by femtosecond pulses," *Phys. Rev. A*, vol. 66, no. 6, p. 062308, 2002, doi: 10.1103/PhysRevA.66.062308.

[7] C. Reimer *et al.*, "Generation of multiphoton entangled quantum states by means of integrated frequency combs," *Science (80-.).*, vol. 351, no. 6278, pp. 1176–1180, 2016, doi: 10.1126/science.aad8532.

[8] A. Vaziri, G. Weihs, and A. Zeilinger, "Experimental Two-Photon, Three-Dimensional Entanglement for Quantum Communication," *Phys. Rev. Lett.*, vol. 89, no. 24, p. 240401, 2002, doi: 10.1103/PhysRevLett.89.240401.

[9] A. Mair, A. Vaziri, G. Weihs, and A. Zeilinger, "Entanglement of the orbital angular momentum states of photons," *Nature*, vol. 412, pp. 313–316, 2001.

[10] G. Molina-Terriza, J. P. Torres, and L. Torner, "Management of the Angular Momentum of Light: Preparation of Photons in Multidimensional Vector States of Angular Momentum," *Phys. Rev. Lett.*, vol. 88, no. 1, pp. 013601–1,4, 2002, doi:

10.1103/PhysRevLett.88.013601.

[11] J. T. Barreiro, N. K. Langford, N. A. Peters, and P. G. Kwiat, “Generation of Hyperentangled Photon Pairs,” *Phys. Rev. Lett.*, vol. 95, no. 26, pp. 260501–1,4, 2005, doi: 10.1103/PhysRevLett.95.260501.

[12] S. Gröblacher, T. Jennewein, A. Vaziri, G. Weihs, and A. Zeilinger, “Experimental quantum cryptography with qutrits,” *New J. Phys.*, vol. 8, no. 75, 2006, doi: 10.1088/1367-2630/8/5/075.

[13] S. Franke-Arnold, S. M. Barnett, M. J. Padgett, and L. Allen, “Two-photon entanglement of orbital angular momentum states,” *Phys. Rev. A - At. Mol. Opt. Phys.*, vol. 65, no. 3, p. 6, 2002, doi: 10.1103/PhysRevA.65.033823.

[14] P. G. Kwiat, E. Waks, A. G. White, I. Appelbaum, and P. H. Eberhard, “Ultrabright source of polarization-entangled photons,” *Phys. Rev. A - At. Mol. Opt. Phys.*, vol. 60, no. 2, pp. R773-76, 1998, doi: 10.1103/PhysRevA.65.063805.

[15] B. Dayan, A. Pe’er, A. A. Friesem, and Y. Silberberg, “Nonlinear Interactions with an Ultrahigh Flux of Broadband Entangled Photons,” *Phys. Rev. Lett.*, vol. 94, no. 4, pp. 043602–1,4, 2005, doi: 10.1103/PhysRevLett.94.043602.

[16] M. Fiorentino, S. M. Spillane, R. G. Beausoleil, T. D. Roberts, P. Battle, and M. W. Munro, “Spontaneous parametric down-conversion in periodically poled KTP waveguides and bulk crystals,” *Opt. Express*, vol. 15, no. 12, p. 7479, 2007, doi: 10.1364/oe.15.007479.

[17] S. M. Lee, H. Kim, M. Cha, and H. S. Moon, “Polarization-entangled photon-pair source obtained via type-II non-collinear SPDC process with PPKTP crystal,” *Opt. Express*, vol. 24, no. 3, p. 2941, 2016, doi: 10.1364/oe.24.002941.

[18] F. Steinlechner *et al.*, “Efficient heralding of polarization-entangled photons from type-0 and type-II spontaneous parametric downconversion in periodically poled KTiOPO_4,” *J. Opt. Soc. Am. B*, vol. 31, no. 9, p. 2068, 2014, doi: 10.1364/josab.31.002068.

[19] M. Fiorentino and R. G. Beausoleil, “Compact sources of polarization-entangled

photons," *Opt. Express*, vol. 16, no. 24, p. 20149, 2008, doi: 10.1364/oe.16.020149.

[20] F. Steinlechner *et al.*, "A high-brightness source of polarization-entangled photons optimized for applications in free space," *Opt. Express*, vol. 20, no. 9, p. 9640, 2012, doi: 10.1364/oe.20.009640.

[21] F. O. Steinlechner *et al.*, "Phase-stable source polarization-entaglement photons in a linear double-pass configuration," *Opt. Express*, vol. 21, no. 10, pp. 11943–11951, 2013, doi: 10.1109/CLEOE-IQEC.2013.6801674.

[22] R. S. Bennink, "Optimal collinear Gaussian beams for spontaneous parametric down-conversion," *Phys. Rev. A*, vol. 81, no. 5, p. 053805, 2010, doi: 10.1103/PhysRevA.81.053805.

[23] D. Ljunggren and M. Tengner, "Optimal focusing for maximal collection of entangled narrow-band photon pairs into single-mode fibers," *Phys. Rev. A*, vol. 72, no. 6, p. 062301, 2005, doi: 10.1103/PhysRevA.72.062301.

[24] X. L. Wang *et al.*, "Experimental ten-photon entanglement," *Phys. Rev. Lett.*, vol. 117, no. 21, pp. 1–6, 2016, doi: 10.1103/PhysRevLett.117.210502.

[25] T. Jennewein, M. Barbieri, and A. G. White, "Single-photon device requirements for operating linear optics quantum computing outside the post-selection basis," *J. Mod. Opt.*, vol. 58, no. 3–4, pp. 276–287, 2011, doi: 10.1080/09500340.2010.546894.

[26] D. J. Griffiths, *Introduction to electrodynamics*, 3rd ed. Prentice-Hall, 1999.

[27] B. E. A. Saleh and M. C. Teich, *Fundamentals of Photonics*. John Wiley & Sons, 1991.

[28] C. Rosales-Guzmán and A. Forbes, *How to Shape Light with Spatial Light Modulators*, 1st ed. SPIE, 2017.

[29] L. Allen, M. W. Beijersbergen, R. J. C. Spreeuw, and J. P. Woerdman, "Orbital angular momentum of light and the transformation of Laguerre-Gaussian laser modes," *Phys. Rev. A*, vol. 45, no. 11, pp. 8185–8189, 1992, doi: 10.1887/0750309016/b1142c6.

[30] A. M. Yao and M. J. Padgett, “Orbital angular momentum: origins, behavior and applications,” *Adv. Opt. Photonics*, vol. 3, no. 2, p. 161, 2011, doi: 10.1364/aop.3.000161.

[31] R. W. Boyd, *Nonlinear Optics*, 3rd ed. Elsevier, 2008.

[32] W. H. Louisell, A. Yariv, and A. E. Siegman, “Quantum fluctuations and noise in parametric processes. I.,” *Phys. Rev.*, vol. 124, no. 6, pp. 1646–1654, 1961, doi: 10.1103/PhysRev.124.1646.

[33] J. P. Gordon, W. H. Louisell, and L. R. Walker, “Quantum fluctuations and noise in parametric processes. II,” *Phys. Rev.*, vol. 129, no. 1, pp. 481–485, 1963, doi: 10.1103/PhysRev.129.481.

[34] J. M. Manley and H. E. Rowe, “Some General Properties of Nonlinear Elements- Part I. General Energy Relations,” *Proc. IRE*, vol. 44, no. 7, pp. 904–913, 1954.

[35] C. Gerry and P. Kneight, *Introductory Quantum Optics*, 1st ed. Cambridge, 2005.

[36] C. K. Hong and L. Mandel, “Theory of parametric frequency down conversion of light,” *Phys. Rev. A*, vol. 31, no. 4, pp. 2409–2418, 1985, doi: 10.1103/PhysRevA.31.2409.

[37] A. Joobeur, B. E. A. Saleh, T. S. Larchuk, and M. C. Teich, “Coherence properties of entangled light beams generated by parametric down-conversion: Theory and experiment,” *Phys. Rev. A - At. Mol. Opt. Phys.*, vol. 53, no. 6, pp. 4360–4371, 1996, doi: 10.1103/PhysRevA.53.4360.

[38] E. Meyer-Scott *et al.*, “Limits on the heralding efficiencies and spectral purities of spectrally filtered single photons from photon-pair sources,” *Phys. Rev. A*, vol. 95, no. 6, 2017, doi: 10.1103/PhysRevA.95.061803.

[39] G. D. Boyd and D. A. Kleinman, “Parametric interaction of focused Gaussian light beams,” *J. Appl. Phys.*, vol. 39, no. 8, pp. 3597–3639, 1968, doi: 10.1063/1.1656831.

[40] T. Guerreiro, A. Martin, B. Sanguinetti, N. Bruno, H. Zbinden, and R. T. Thew, “High efficiency coupling of photon pairs in practice,” *Opt. Express*, vol. 21, no. 23, pp.

27641–51, 2013, doi: 10.1364/oe.21.027641.

[41] M. Mirhosseini, O. S. Magana-Loaiza, C. Chen, B. Rodenburg, M. Malik, and R. W. Boyd, “Rapid generation of light beams carrying orbital angular momentum,” *Opt. Express*, vol. 21, no. 25, pp. 30204–30211, 2013, doi: 10.1364/oe.21.030204.

[42] S. Ngcobo, I. Litvin, L. Burger, and A. Forbes, “A digital laser for on-demand laser modes,” *Nat. Commun.*, vol. 4, pp. 1–6, 2013, doi: 10.1038/ncomms3289.

[43] M. W. Beijersbergen, L. Allen, H. E. L. O. van der Veen, and J. P. Woerdman, “Astigmatic laser mode converters and transfer of orbital angular momentum,” *Opt. Commun.*, vol. 96, no. 1,2,3, pp. 123–132, 1993, doi: 10.1887/0750309016/b1142c21.

[44] L. Marrucci *et al.*, “Spin-to-orbital conversion of the angular momentum of light and its classical and quantum applications,” *J. Opt.*, vol. 13, no. 6, p. 064001, 2011, doi: 10.1088/2040-8978/13/6/064001.

[45] G. C. G. Berkhout, M. P. J. Lavery, J. Courtial, M. W. Beijersbergen, and M. J. Padgett, “Efficient sorting of orbital angular momentum states of light,” *Phys. Rev. Lett.*, vol. 105, no. 15, p. 153601, 2010, doi: 10.1103/PhysRevLett.105.153601.

[46] G. Labroille, P. Jian, N. Barre, B. Denolle, and J. F. Morizur, “Mode selective 10-mode multiplexer based on multi-plane light conversion,” 2016, doi: 10.1364/ofc.2016.th3e.5.

[47] E. Noponen and J. Turunen, “Complex-amplitude modulation by high-carrier-frequency diffractive elements,” *J. Opt. Soc. Am. A*, vol. 13, no. 7, p. 1422, 1996, doi: 10.1364/josaa.13.001422.

[48] E. Bolduc, N. Bent, E. Santamato, E. Karimi, and R. W. Boyd, “Exact solution to simultaneous intensity and phase encryption with a single phase-only hologram,” *Opt. Lett.*, vol. 38, no. 18, p. 3546, 2013, doi: 10.1364/ol.38.003546.

[49] G. Labroille, B. Denolle, P. Jian, P. Genevaux, N. Treps, and J.-F. Morizur, “Efficient and mode-selective spatial multiplexer based on multi-plane light conversion,” *Opt. Express*, vol. 22, no. 13, pp. 15599–15607, 2014, doi: 10.1364/oe.22.015599.

[50] N. K. Fontaine, R. Ryf, H. Chen, D. T. Neilson, K. Kim, and J. Carpenter, "Laguerre-Gaussian mode sorter," *Nat. Commun.*, vol. 10, pp. 1–7, 2019, doi: 10.1038/s41467-019-09840-4.

[51] W. Han, Y. Yang, W. Cheng, and Q. Zhan, "Vectorial optical field generator for the creation of arbitrarily complex fields," *Opt. Express*, vol. 21, no. 18, pp. 20692–20706, 2013, doi: 10.1364/oe.21.020692.

[52] B. Franz and H. Bülow, "Mode Group Division Multiplexing in Graded-Index Multimode Fibers," *Bell Labs Tech. J.*, vol. 18, no. 3, pp. 153–172, 2013, doi: 10.1002/bltj.